

Topology Optimization of Micro Piezoelectric Actuators and Energy Harvesters at Femto-St Institute: Summary and MATLAB Code Implementation

Abbas Homayouni-Amlashi^{1*}, Thomas Schlinquer^{1,2}, Peter Kipkemoi^{1,3},
Jean Bosco Byiringiro³, Micky Rakotondrabe⁴, Michael Gauthier¹,
Abdenbi Mohand-Ousaid¹

¹AS2M Department, Université de Franche-Comté, SUPMICROTECH, CNRS, Institut FEMTO-ST, Besançon, 25000, France.

²ESEO engineering school, Dijon, 21231, France.

³Department of Mechatronics Engineering, Dedan Kimathi University of Technology, Nyeri, Kenya.

⁴LGP laboratory, National School of Engineering in Tarbes (ENIT-INPT), University of Toulouse, Tarbes, 65000, France.

*Corresponding author(s). E-mail(s): abbas.homayouni_amlashi@univ-fcomte.fr;

Abstract

This paper primarily summarize the research efforts conducted within the AS2M department of the FEMTO-ST institute, focusing on topology optimization of piezoelectric structures. In this regard, the principles and the possibilities offered by topology optimization with a specific emphasis on the SIMP approach (Solid Isotropic Material with Penalization) are highlighted. The design processes of piezoelectric micro-actuators and energy harvesters are described, The optimized piezoelectric structures are presented and the improvements over classical designs are assessed. Moreover, in this paper, we present the eigenvalue optimization of the piezoelectric energy harvester by tuning the mass of attachment as an optimization variable. The theoretical development is accompanied by the developed MATLAB code to implement the topology optimization algorithm. This code is the update and extension of the previously published codes by authors for piezoelectric structures while it will be the first published code of its kind that considers the tuning of the natural frequency of the piezo structure. Finally, the paper discusses the feasibility and the potential of multi-material topology optimization.

Keywords: Piezoelectric micro-actuator, piezoelectric energy harvester, topology optimization, Matlab code

1 Introduction

The interest of miniaturized systems is considerable and well established [1]. Based on smart materials like piezoelectric materials, they can change their inherent properties in response to

external stimuli in a controllable manner. Taking this advantage, they are widely used in several applications such as: biomedical, optics, fluidics, car industry, energy harvesting, electronics, etc. However, due to their size and density of integration, their design remains challenging because it

001
002
003
004
005
006
007
008
009
010
011
012
013
014
015
016
017
018
019
020
021
022
023
024
025
026
027
028
029
030
031
032
033
034
035
036
037
038
039
040
041
042
043
044
045
046
047
048
049
050
051

052 requires taking into account the coupling between
053 the structure and its mechanisms through a global
054 design strategy. This requirement is induced by
055 smart materials that play a significant role in the
056 technological design of these systems. To address
057 this challenge, various design methodologies have
058 been proposed such as optimal arrangement of
059 actuators/sensors [2–4], interval method [5, 6] or
060 blocks method [7, 8]. Nevertheless, most of these
061 methods lack generalization since they act only
062 on the geometric parameters of the structure.
063 This limits efficient shape design of the active
064 mechanisms (actuation and measurement) and
065 consequently that of the resulting structure.

066 In this regard, topology optimization [9], and
067 particularly the SIMP (Solid Isotropic Mate-
068 rial with Penalization) method seems to be a
069 promising solution. Unlike classical optimization
070 methods, it gives rise to efficient structures in
071 response to requirement specifications. Its princi-
072 ple is mainly based on optimal material distribu-
073 tion within a specified design domain. Presented
074 initially by Sigmund et al. [9–11], this powerful
075 method is suitable for the design of passive struc-
076 tures. Since becoming a conceptual design tool,
077 it has been particularly applied to design smart
078 structures based on piezoelectric materials [12].
079 However, it remains challenging to handle due to
080 the non-intuitive and non-unified integration of
081 piezoelectric materials.

082 To tackle this limitation, the AS2M depart-
083 ment has been actively working since 2018 to
084 enhance the SIMP method by extending it to
085 include piezoelectric materials. The objective is
086 to provide a straightforward strategy for inte-
087 grating the physics of the piezoelectric materials
088 within the SIMP method. This gave rise to sev-
089 eral challenges related to: smart materials mod-
090 eling, finite-elements formulation, computational
091 and numerical implementation. All these chal-
092 lenges have been or are being investigated at
093 AS2M/FEMTO-ST institute.

094 This paper provides first a comprehensive sum-
095 mary of the research that has been conducted
096 at the AS2M department/FEMTO-ST institute,
097 the works that are currently underway, and the
098 potential directions for future advancements con-
099 cerning the design of piezoelectric actuators and
100 energy harvesters. Secondly, [we present topology
101 optimization of piezoelectric energy harvesters in
102 which the natural frequency of the structure will](#)

[be tuned with the help of considering the Mass
of attachment as an optimization variable. The
theoretical aspects in this regard are accompanied
by the implementation MATLAB code.](#) The pro-
vided MATLAB code is the development of the
previously published codes by author for topology
optimization of piezoelectric structures [13] that
were the first topology optimization MATLAB
codes published in the area of piezoelectricity.
All the MATLAB codes published in the litera-
ture for topology optimization in different physics
are reviewed in [14]. The published code in this
paper will be the first published MATLAB code in
the area of topology optimization of piezoelectric
structure with frequency tuning.

In the last part of the paper, we discuss the
possibility of multi material topology optimization
in which both active (piezo) and passive material
will be developed and optimized to obtain more
efficient designs.

2 Topology optimization

2.1 SIMP approach

Topology optimization and in particular the SIMP
approach is a mathematical design methodology
aiming to find an optimal layout within a limited
design domain [9]. Based on material distribu-
tion, the method allows minimizing or maximiz-
ing an objective function while subjected to one
or several constraints. Its key principle consists
of introducing a density penalization law. The
method is largely integrated into several design
softwares such as COMSOL, ALTAIR Inspire,
Ansys Discovery, SOLIDWORKS, etc. As a global
and systematic approach, it is largely used in
the engineering and design of passive mechan-
ical structures because it offers several advantages
such as weight reduction while enhancing perfor-
mance and efficiency.

The method has also been applied for the topo-
logical design of active structures in particular
piezoelectric structures [12]. However, the existing
methodology lacks some mathematical develop-
ment regarding the optimization of the polarity
in addition to the topology. These mathemati-
cal limitations include the explicit formulation of
the sensitivity analysis. Moreover, the realization
of the optimized topologies of the piezoelectric
structures received a very little attention in the

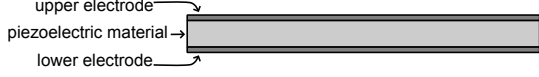


Fig. 1 Piezoelectric material sandwiched between two electrodes.

literature. We addressed these limitations by (i) developing analytical and theoretical aspects of topology optimization of piezoelectric structures, (ii) developing algorithms and computer codes and (iii) fabricating and investigating experimentally the obtained structures. The common underlying factors in these developments were piezoelectric material modeling and numerical implementation.

2.2 Piezoelectric modeling

Our primary investigations focused on planar piezoelectric structures. Thus, the starting design domain consists of a piezoelectric layer sandwiched between two electrodes as illustrated in Fig. 1. Its modeling involves several simplifying assumptions [15, 16] including plan-stress assumption which enable us to derive a 2D model from the IEEE 3D model [17] of piezoelectric material. To discretize the design domain and obtain the finite element modeling, the four-node rectangular element is employed as shown in Fig. 4-(a). With discretization of the design domain, the global finite element equilibrium equation can be derived as [18]

$$\begin{bmatrix} M & 0 \\ 0 & 0 \end{bmatrix} \begin{bmatrix} \ddot{U} \\ \ddot{\Phi} \end{bmatrix} + \begin{bmatrix} K_{uu} & K_{u\phi} \\ K_{\phi u} & -K_{\phi\phi} \end{bmatrix} \begin{bmatrix} U \\ \Phi \end{bmatrix} = \begin{bmatrix} F \\ Q \end{bmatrix} \quad (1)$$

where U and ϕ are the vectors of the mechanical displacement and electric potential respectively. F and Q are the applied external mechanical force and electrical charge. M , K_{uu} , $K_{u\phi}$, $K_{\phi\phi}$ are the global mass matrix, mechanical stiffness matrix, piezoelectric coupling matrix and piezoelectric permittivity matrix respectively. The global matrices are formed by assembling the elemental matrices [13]. The global equilibrium equation (1) can be normalized to avoid the numerical instabilities and can be re-written based on the normalization which is provided in Ref. [13]. The normalization starts by factorizing the highest value of each elemental matrix,

$$\begin{aligned} \tilde{k}_{uu} &= k_{uu}/k_0, & \tilde{k}_{u\phi} &= k_{u\phi}/\alpha_0 \\ \tilde{k}_{\phi\phi} &= k_{\phi\phi}/\beta_0, & \tilde{m} &= m/m_0 \end{aligned} \quad (2)$$

where $k_0, \alpha_0, \beta_0, m_0$ are the highest values of the corresponding matrices. Then, the new FEM equation for piezoelectric actuator, can be written as

$$\tilde{K}_{uu}\tilde{U} + \tilde{K}_{u\phi}\tilde{\Phi} = \tilde{F} \quad (3)$$

In equation (3), $(\tilde{\cdot})$ stands for the normalized quantities and

$$\begin{aligned} \tilde{F} &= F/f_0, & \tilde{U} &= U/u_0, & \tilde{\Phi} &= \Phi/\phi_0 \\ u_0 &= f_0/k_0, & \phi_0 &= f_0/\alpha_0 \end{aligned} \quad (4)$$

and the new FEM equation for energy harvesting is derived as

$$\begin{bmatrix} \tilde{K}_{uu} - \tilde{M}\tilde{\Omega}^2 & \tilde{K}_{u\phi} \\ \tilde{K}_{\phi u} & -\gamma\tilde{K}_{\phi\phi} \end{bmatrix} \begin{bmatrix} \tilde{U} \\ \tilde{\Phi} \end{bmatrix} = \begin{bmatrix} \tilde{F} \\ 0 \end{bmatrix} \quad (5)$$

where

$$\tilde{\Omega}^2 = \Omega^2 m_0/k_0, \quad \gamma = k_0\beta_0/\alpha_0^2 \quad (6)$$

In equation (5), B is a Boolean matrix to apply the equipotential condition on the electrodes with dimension $N_e \times N_P$ where N_e is the number of nodes and N_P is the number of potential electrodes where for 2D case $N_P = 1$. $\tilde{\Omega}$ is the normalized excitation frequency (Ω), V_p is the generated voltage by mechanical vibration and γ is the normalized factor that keeps the solution of the system equal before and after applying the normalization.

After solving the FEM, we need to rollback the normalization and calculate the real outputs of the system (i.e. ϕ and U). In actuation mode, the input of the system is potential and hence the value of Φ_0 is assumed by user a priori. As such, the real value of displacement can be calculated by

$$U = U_0\tilde{U} = \Phi_0\alpha_0\tilde{U}/k_0 \quad (7)$$

In the energy harvesting case, the force is the input and the value of f_0 is assumed by user a

154 priory. Therefore, the real value of potential can
 155 be calculated by

156

157

158

$$\Phi = \Phi_0 \tilde{\Phi} = f_0 \Phi / \alpha_0 \quad (8)$$

159

160

161

162

With the developed finite element model, it is possible to formulate the optimization problem for piezoelectric actuators and energy harvesters.

163

164

3 Piezoelectric micro-actuators

165

166

167

168

169

170

171

172

173

174

175

176

177

178

179

180

181

182

183

184

185

186

187

188

189

190

191

192

193

The use of piezoelectric materials to actuate microbotics systems is of particular interest. As a smart material, they have several advantages such as: high displacement resolution, large output force, high dynamics response and significant scaling-down possibilities [19]. However, due to their crystalline arrangement, they provide a low relative deformation (0.1% of actuator's size) that limits their stroke [20]. To overcome this limitation, we employed topology optimization framework [16] to optimize both the topology and the polarity of the actuator. This simultaneous optimization allows combining material expansion and compression in order to increase the stroke of the actuator without using any passive amplification mechanism. This enables the miniaturization of the optimal design. Two 1D actuators were designed starting from a full domain considered as a basic reference piezoelectric actuator. The first design considered only the optimization of topology while the second one took into account the optimization of the topology and polarization profile simultaneously. This section recaps the problem formulation, the optimization and the main results of this study. To find out more theoretical details, readers can refer to [15, 16].

194

3.1 Problem formulation

195

196

197

198

199

200

201

202

203

204

To formulate the topology optimization problem, we use the SIMP (Solid Isotropic Material with Penalization) approach. In this approach, optimization variables are attributed to each element in the design domain to relax the physical properties from binary values to continuous values [21]. The extension of SIMP approach for piezoelectric materials known as "Piezoelectric Material with

Penalization and Polarization (PEMAP-P)" can be expressed as follows [22, 23]:

$$\begin{aligned} \tilde{k}_{uu}(x) &= (E_{min} + x^{p_{uu}}(E_0 - E_{min})) \tilde{k}_{uu} \\ \tilde{k}_{u\phi}(x, P) &= (e_{min} + x^{p_{u\phi}}(e_0 - e_{min}))(2P - 1)^{p_P} \tilde{k}_{u\phi} \\ \tilde{k}_{\phi\phi}(x) &= (\varepsilon_{min} + x^{p_{\phi\phi}}(\varepsilon_0 - \varepsilon_{min})) \tilde{k}_{\phi\phi} \\ \tilde{m}(x) &= x \tilde{m} \end{aligned} \quad (9)$$

where E_{min} , e_{min} and ε_{min} are small numbers to define the minimum values for stiffness, coupling and dielectric matrices while E_0 , e_0 and ε_0 are equal to one to define the maximum values of the respected matrices. The definition of minimum values are provided to avoid the singularities during the optimization iterations. x is the density ratio of each element which has a value between zero and one. P is the polarization variable which also has the value between zero and one and determines the direction of polarization. p_{uu} , $p_{u\phi}$, $p_{\phi\phi}$ and p_P are penalization coefficients for the stiffness, coupling, dielectric matrices and polarization value respectively. It is obvious that in equation (9), the normalized form of piezoelectric matrices are used. However, the interpolation function is true for non-normalized matrices as well.

Now, the optimization problem can be formulated by definition of objective function, constraints and optimization variables. The objective function can be defined using the compliant mechanism analysis in which the goal is to maximize the deflection of a structure in a particular direction. Different objective functions can be considered for compliant mechanisms which are reviewed in [24]. Here, a simple objective function is chosen with a modeled spring to simulate the stiffness of the target object as it is illustrated in the Fig. 2-(a). Moreover, a constraint on the volume of the material can be defined to minimize the consumed material and to increase the flexibility of structure in favor of higher displacement. The optimization variables also defined in the material interpolation scheme (9). Therefore, the optimization problem for piezoelectric micro-actuators can be formulated as follows

$$\text{minimize } J_{act} = -L^T \tilde{U}$$

$$\begin{aligned}
\text{Subject to } V(x) &= \sum_{i=1}^{NE} x_i v_i \leq V \\
0 &< x_i \leq 1 \\
0 &\leq P_i \leq 1
\end{aligned} \tag{10}$$

where L is a Boolean vector with a value of one that corresponds to the output displacement node and zero otherwise. V is the target volume which is a fraction of the overall volume of the design domain while v_i is the volume of each element and NE is the total number of elements and i is the number of each element in the design domain.

3.2 Sensitivity analysis

To solve the optimization problem, we use the gradient based solvers like Optimality Criteria (OC) and method of moving asymptotes (MMA) [25, 26]. As such, the sensitivity of objective function with respect to optimization variables should be calculated. Based on the material interpolation scheme (9), we have two optimization variables known as density (x) and polarization (P). The sensitivity with respect to (x) is calculated by using the adjoint method as

$$\frac{\partial J}{\partial x_i} = \lambda_i^T \frac{\partial \tilde{k}_{uu}}{\partial x_i} \tilde{u}_i + \lambda_i^T \frac{\partial \tilde{k}_{u\phi}}{\partial x_i} \tilde{\phi}_i \tag{11}$$

where λ is the adjoint vector at elemental level. λ is introduced to avoid taking the derivative of displacement with respect to design variable i.e. $\frac{\partial \tilde{u}_i}{\partial x}$. The sensitivity with respect to polarization is

$$\frac{\partial J}{\partial P_i} = \lambda_i^T \frac{\partial \tilde{k}_{u\phi}}{\partial P_i} \tilde{\phi}_i \tag{12}$$

The following adjoint equation should be solved to find the adjoint vectors,

$$-L^T + \Lambda^T \tilde{K}_{uu} = 0 \tag{13}$$

Where Λ is the adjoint vector at system level (global level).

Based on equations (11) and (12), the derivative of piezoelectric stiffness and coupling matrices with respect to design variables are required which can be derived with the help of equation (9) as

$$\begin{aligned}
\frac{\partial \tilde{k}_{uu}}{\partial x_i} &= p_{uu}(E_0 - E_{min})x_i^{p_{uu}-1} \tilde{k}_{uu} \\
\frac{\partial \tilde{k}_{u\phi}}{\partial x_i} &= p_{u\phi}(e_0 - e_{min})x_i^{p_{u\phi}-1} (2P_i - 1)^{p_P} \tilde{k}_{u\phi}
\end{aligned} \tag{14}$$

$$\frac{\partial \tilde{k}_{u\phi}}{\partial P_i} = 2p_P(e_0 - e_{min})(2P_i - 1)^{p_P-1} x_i^{p_{u\phi}} \tilde{k}_{u\phi} \tag{15}$$

When the sensitivity analysis is provided, the SIMP algorithm can be developed. Beforehand, the design domain and application should be defined.

3.3 Definition of design domain and application

Figures 2-(a,b) illustrates the definition and the mechanical formulation of 1D piezoelectric actuator. The bottom side of the domain is clamped while the middle point of the top side is considered as the actuator output. In addition, the actuator-object interaction is modeled as a spring that modulates the actuator displacement: a lower stiffness value results in a higher displacement and vice versa. Using this configuration, two optimized designs are obtained where the difference lies in whether or not the polarization is optimized. In both cases, the volume fraction is set to 0.3, meaning that only 30% of the initial domain is used for the optimized designs.

After performing the sensitivity analysis, and defining the constraint, the topology optimization algorithm can be implemented.

3.4 Algorithm, optimization and simulation

Following the modeling and formulation of the problem, an optimization algorithm was developed and implemented under MATLAB [15]. The application of this algorithm leads to the designs depicted in Figs. 2-(c,e). Layout (c) comprises a uniform electrode while layout (e) comprises two different electrodes with opposite polarities. The second design comprises two regions with inverse polarities. When one region retracts the other

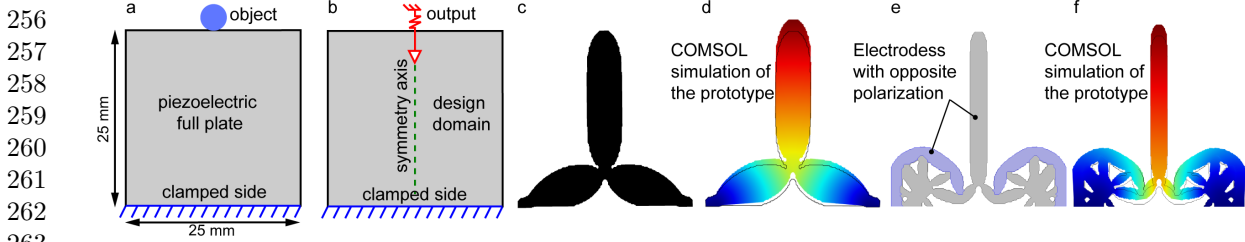


Fig. 2 Topology optimization of a piezoelectric micro-actuators. a) Problem definition, b) Problem formulation, c) Optimized layout without polarity, d) Simulated layout without polarity, e) Optimized layout with polarity, f) Simulated layout with polarity.

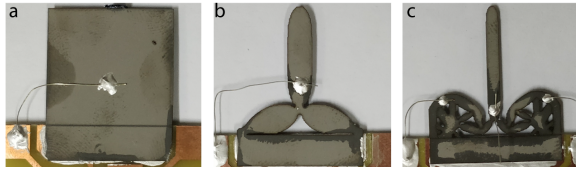


Fig. 3 Fabricated prototypes, a) Full plate (reference actuator), b) Prototype without polarity optimization, c) Prototype with polarity optimization.

extends resulting in a considerable improvement of output displacement. This analysis is confirmed by FEA simulations illustrated in Figs. 2-(d,f) where the obtained results show that the displacement of the design with optimized polarity is almost twice the displacement of the design with uniform polarity. More comparison results between the full actuator plate (reference actuator) and the optimized designs are reported in Table 1.

3.5 Fabrication and experimental validation

Starting from a piezoelectric plate, the three prototypes shown in Fig. 3 were fabricated. The fabrication process started by cutting the designs from piezoelectric plates (commercial piezoelectric material PSI-5H4E from Piezo Systems Inc) using a laser machine (Siro Lasertec GmbH, Pforzheim, Germany). Then, the wires are glued to the electrodes of the PZT plates. Moreover, to follow the polarization profile, the top electrode is divided into two sections to avoid charge cancellation. An experimental bench was set and a series of measurements were performed under a maximum excitation voltage of 5V which respects the linear assumption of the piezoelectric model. The resulting average displacements are reported in

Table 1. As expected, there is a satisfying agreement between the experimental and the simulation results. In addition, the superiority of the optimized designs versus the full piezoelectric plate in terms of stroke is observed.

3.6 Discussion

The developed algorithm reduces drastically the material amount while enhancing the actuator energy density and stroke. Indeed, only 30% of the material was optimally distributed in order to provide a displacement greater than the displacement of an actuator with a uniform polarization. Although the actuator output force decreased, the optimization led to a compact and economical design. This is particularly interesting in the context of miniaturization since the non-occupied space can be utilized to implement additional functionalities such as sensors or electronic circuits.

4 Piezoelectric energy harvesters

In parallel to actuation, piezoelectric materials are widely used in energy harvesting applications. Converting vibration to electrical energy, these devices, i.e, Piezoelectric Energy Harvesters (PEHs) offer a potential alternative to batteries in low-power-wireless devices such as wireless sensors [27], small-scale robots [28], etc. Thanks to the direct effect of piezoelectricity, they can convert mechanical to electrical energies with a simple mechanism. This simplicity makes the piezoelectric energy harvester more efficient than their rivals like electromagnetic and triboelectric at small scales. At AS2M department, we mainly worked on the optimization of the mechanical structures of PEHs.

Table 1 Summary of simulation and experimental results [16]

	Simulation (Input voltage = 5V)		
	Full plate	Opt without pol	Opt with pol
Displacement (nm/V)	57	81	161
Displacement gain w.r.t.f.p	-	1.42	2.82
Blocking force (N)	2.56	0.21	0.18
Blocking force gain w.r.t.f.p	-	0.08	0.07
Energy density (J/m^3)	4.55	1.81	3.10
Energy density gain w.r.t.f.p	-	0.39	0.68

	Experiment (Input voltage = 5V)		
	Full plate	Opt without pol	Opt with pol
Displacement (nm/V)	62	86	174
Displacement gain w.r.t.f.p	-	1.38	2.8

* w.r.t.f.p : with respect to full plate

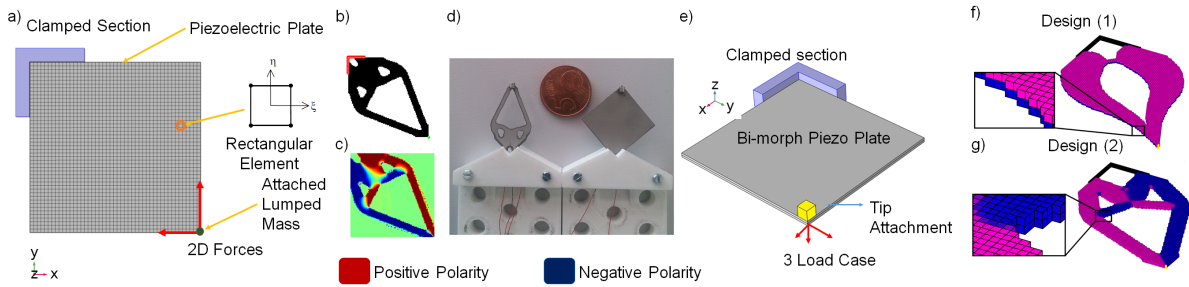


Fig. 4 Piezoelectric Energy Harvesters designed by topology optimization. a) single-layer piezo plate modeled by 2D finite element method [29]. b) Optimized topology, c) Optimized polarity, d) Fabricated prototype, e) Bi-morph piezo plate modeled by 3D finite element method [30], f) Optimized topology without polarization optimization, g) Optimized topology with polarization optimization

Mostly known and still used configuration for the vibrational PEH is the cantilever configuration with tip attachment due to its largely produced strains and feasibility of fabrication. Considering this configuration as the first approach to increase the efficiency of the cantilever PEH, we proposed to have in-span attachments in addition to tip attachment in order to harvest the energy from higher modes and resonance frequencies [31]. Based on an analytical approach to find the output voltage, we proposed a neural network-based genetic algorithm (GA) approach to optimize the placement and geometry of the in-span attachments. However, the major problem with cantilever configuration is that it is one degree of freedom configuration, which can absorb the energy from one direction of excitation. This will restrict the possible applications of the cantilever PEHs, where the excitation can come from different directions. There are some

designs for multi-directional PEHs in the literature [32, 33]. However, the miniaturization of these mechanism-based designs is challenging. To tackle this problem, we employed SIMP topology optimization to obtain new and previously unknown configurations for the PEH.

4.1 Single-layer piezoelectric energy harvester

4.1.1 Modeling & problem formulation

Utilizing the piezoelectric constitutive equations, first, a 2D finite element model of a single piezoelectric plate sandwiched between two electrodes (Fig. 1) is developed. The plan-stress assumption is employed to derive the constitutive equation. The normalized equilibrium equation is mentioned in equation (5).

358 TO formulate the problem, objective function
 359 is defined as the weighed sum of the mechanical
 360 and electrical energy. Similar to actuation case, a
 361 constraint is defined on the volume of the mate-
 362 rial and optimization variables are considered as
 363 density and polarization. Therefore, the problem
 364 is formulated as follows,

$$\begin{aligned}
 & \text{minimize } J_{EH} = w_j \Pi^S - (1 - w_j) \Pi^E \\
 & \text{Subject to } V(x) = \sum_{i=1}^{NE} x_i v_i \leq V \\
 & \quad 0 < x_i \leq 1 \\
 & \quad 0 \leq P_i \leq 1
 \end{aligned} \tag{16}$$

374 Π^E and Π^S are electrical and mechanical ener-
 375 gies respectively which are defined in the following
 376 form [22, 34]

$$\begin{aligned}
 \Pi^S &= \left(\frac{1}{2}\right) \tilde{U}^T \overline{K_{uu}} \tilde{U}, \quad \Pi^E = \left(\frac{1}{2}\right) V_p^T \overline{K_{\phi\phi}} V_p \\
 \overline{K_{uu}} &= \left[\tilde{K}_{uu} - \tilde{M} \tilde{\Omega}^2 \right]_{bc}, \quad \overline{K_{\phi\phi}} = \gamma B^T \tilde{K}_{\phi\phi} B
 \end{aligned} \tag{17}$$

384 In optimization equation (16), w_j is the weigh-
 385 ing factor which has the value between 0 and 1 and
 386 will be found by using trial and error approach.
 387 The basis for choosing this value can be the max-
 388 imum energy conversion factor of the plate under
 389 the same force.

392 4.2 Sensitivity analysis

393 After defining the mechanical and electrical ener-
 394 gies, the sensitivity of each energy with respect to
 395 density ratio x can be found as [29, 30, 34]

$$\begin{aligned}
 \frac{\partial \Pi^S}{\partial x_i} &= \left(\frac{1}{2}\right) \tilde{u}_i^T + \lambda_{1,i}^T \frac{\partial(\tilde{k}_{uu} - \tilde{m} \tilde{\Omega}^2)}{\partial x_i} \tilde{u}_i + \\
 & \lambda_{1,i}^T \frac{\partial \tilde{k}_{u\phi}}{\partial x_i} \tilde{\phi}_i + \mu_{1,i}^T \frac{\partial \tilde{k}_{\phi u}}{\partial x_i} \tilde{u}_i - \mu_{1,i}^T \frac{\gamma \partial \tilde{k}_{\phi\phi}}{\partial x_i} \tilde{\phi}_i
 \end{aligned} \tag{18}$$

$$\frac{\partial \Pi^E}{\partial x_i} = \frac{1}{2} \tilde{\phi}_i^T \frac{\gamma \partial \tilde{k}_{\phi\phi}}{\partial x_i} \tilde{\phi}_i - \mu_{2,i}^T \frac{\gamma \partial \tilde{k}_{\phi\phi}}{\partial x_i} \tilde{\phi}_i +$$

$$\lambda_{2,i}^T \frac{\partial(\tilde{k}_{uu} - \tilde{m} \tilde{\Omega}^2)}{\partial x_i} u_i + \lambda_{2,i}^T \frac{\partial \tilde{k}_{u\phi}}{\partial x_i} \tilde{\phi}_i + \mu_{2,i}^T \frac{\partial \tilde{k}_{\phi u}}{\partial x_i} \tilde{u}_i \tag{19}$$

in which μ and λ are the elemental adjoint vec-
 tors which are calculated by the following global
 coupled system

$$\begin{aligned}
 \begin{bmatrix} \overline{K_{uu}} & \overline{K_{u\phi}} \\ \overline{K_{\phi u}} & -\overline{K_{\phi\phi}} \end{bmatrix} \begin{bmatrix} \Lambda_1 \\ \Upsilon_1 \end{bmatrix} &= \begin{bmatrix} -\overline{K_{uu}} \tilde{U} \\ 0 \end{bmatrix} \\
 \begin{bmatrix} \overline{K_{uu}} & \overline{K_{u\phi}} \\ \overline{K_{\phi u}} & -\overline{K_{\phi\phi}} \end{bmatrix} \begin{bmatrix} \Lambda_2 \\ \Upsilon_2 \end{bmatrix} &= \begin{bmatrix} 0 \\ -\overline{K_{\phi\phi}} V_p \end{bmatrix}
 \end{aligned} \tag{20}$$

where Λ and Υ , are the global adjoint vectors
 which need to be disassembled to form the elemental
 adjoint vectors

$$[\lambda_1]_{bc} = \Lambda_1, [\lambda_2]_{bc} = \Lambda_2, [\mu_1] = B \Upsilon_1, [\mu_2] = B \Upsilon_2 \tag{21}$$

Now, the sensitivities with respect to polariza-
 tion (P) is calculated as well [29, 30]

$$\begin{aligned}
 \frac{\partial \Pi^S}{\partial P_i} &= \lambda_{1,i}^T \frac{\partial \tilde{k}_{u\phi}}{\partial P_i} \tilde{\phi}_i + \mu_{1,i}^T \frac{\partial \tilde{k}_{\phi u}}{\partial P_i} \tilde{u}_i \\
 \frac{\partial \Pi^E}{\partial P_i} &= \lambda_{2,i}^T \frac{\partial \tilde{k}_{u\phi}}{\partial P_i} \tilde{\phi}_i + \mu_{2,i}^T \frac{\partial \tilde{k}_{\phi u}}{\partial P_i} \tilde{u}_i
 \end{aligned} \tag{22}$$

Based on sensitivity equations in (19) and (22),
 the derivative of all piezoelectric matrices with
 respect to the design variables are required. The
 derivative of stiffness and coupling matrices are
 found in equations (14) and (15). Here, the deriva-
 tive of dielectric matrix and mass matrix is also
 required which are

$$\begin{aligned}
 \frac{\partial \tilde{k}_{\phi\phi}}{\partial x_i} &= p_{\phi\phi} (\varepsilon_0 - \varepsilon_{min}) x_i^{p_{\phi\phi}-1} \tilde{k}_{\phi\phi} \\
 \frac{\partial \tilde{m}}{\partial x_i} &= \tilde{m}_i
 \end{aligned} \tag{23}$$

In addition to derivative of piezoelectric matri-
 ces with respect to density, derivation of the piezo-
 electric coupling matrix with respect to polariza-
 tion variable is also required

$$\frac{\partial \tilde{k}_{u\phi}}{\partial P_i} = 2p_P(2P_i - 1)^{p_P-1} x_i^{p_{u\phi}} \tilde{k}_{u\phi} \quad (24)$$

After calculation of sensitivities, the optimization variables can be updated in each iteration of optimization with the help of gradient-based optimizers like optimality criteria (OC) and Method Moving Asymptotes (MMA) [26].

For the single layer piezoelectric plate, the goal is to design a two degrees of freedom energy harvester that can harvest the energy from external in-plane harmonic force coming from different directions. In this regard, the configuration of load and boundary conditions in Fig. 4-(a) is proposed. The most challenging problem in this case is the charge cancellation due to a combination of tension and compression in different parts of the plate. However, optimization of polarization profile overcomes the problem of charge cancellation. Moreover, low volume fraction (optimized design volume/full plate volume) decreases the stiffness of the piezoelectric plate against in-plane forces.

4.2.1 Numerical results, simulation & experiment

In panels (b) and (c) of the same figure, the final optimized layout and polarization profile for PZT plate under excitation of two harmonic forces in two directions can be seen [29]. In panel (c), the red color and blue color represent positive and negative polarization in the z direction.

To analyze the performance of the optimized design, COMSOL multiphysics is used to compare the performance of the optimized design with the full plate. The simulation results proved the superiority of the optimized designs over the classical full plate while having less amount of material [29]. On the other hand, the amount of produced voltage and electrical power is not the same for every direction of the force. This is due to the fact that the stiffness of the plate in different directions is not the same. For the sake of brevity, we do not present the simulation results here. Interested readers are referred to the published paper [29].

The fabrication process is similar to what has been explained for the piezoelectric actuators. The difference here is that magnets are attached at the

tip of the beam to generate vibrations force when excited by an electromagnet as it is shown in figure 4-(d). The magnets are attached in two different directions so they can excite the designs in two different directions.

Experimental results demonstrated that for an excitation frequency equal to 20 Hz, the voltage and power of the optimized design are 8.75 and 7.54 times higher than the full plate. These improvements are due to the fact that the optimized design is having better strain distribution and more importantly, it has separated electrodes that avoid charge cancellation.

4.3 Bi-morph piezoelectric energy harvester

In the next phase of our research, a bi-morph piezoelectric plate instead of the single-layer piezoelectric plate is considered as a design domain to consider out-of-plane forces and deformations [30].

4.3.1 Modeling & problem formulation

Similar objective and constraints from single-layer PEH are considered in the optimization problem of the multi-directional Bi-morph PEH i.e. reduction of weight while maximizing the efficiency of the harvested energy from excitation coming from different directions. In the case of bi-morph PEH, the configuration of the boundary condition remains the same while a 3-load case is applied at the tip of the structure (Fig. 4-(e)). The bi-morph plate consists of 3 electrodes on the top, middle and bottom surfaces of the plate. The finite element modeling of the system is done by discretizing the design domain with a finite number of 3D hexahedron elements.

4.3.2 Algorithm & optimization

The sensitivity analysis and optimization algorithm for 3D and 2D finite element modeling is formulated similarly. However, the implementation MATLAB code changes considerably to include the third dimension and application of electrical boundary conditions regarding the existence of several electrodes.

4.3.3 Numerical results, simulation & experiment

The results of the optimization for two cases are shown in Fig. 4-(f,g) [30]. The optimized design (1) is the result of optimization without optimizing the polarity and design (2) is the result of optimization with optimizing polarity. In design (1), in the case of planar forces, there will be charge cancellation due to compression and tension in different parts of the layer. To remedy, in design (2), the polarity is optimized as well. For the realization of this polarization profile, the top and bottom electrodes are divided into two sections to simulate the polarization profile. As such, the design has 2 electrodes on top, 2 electrodes on bottom and one electrode in the middle.

To assess experimentally the performance of the optimized designs, their electrical to mechanical efficiency is compared with a classical full plate. By COMSOL simulation, we demonstrated how the designs harvested the energy coming from different excitation in 3D space and the superiority of the optimized designs over the full piezoelectric plate is demonstrated. The experimental investigation demonstrated that the optimized design with optimized polarity can have up to 2 times better voltage output than the piezoelectric full plate while having less amount of mass [30].

Finally, although optimized designs are multi-directional harvesters, but they are not excited at their resonance frequency. This is considered in the next stage of our research.

4.4 Frequency tuning & optimization of mass

The best efficiency of a vibrational PEH can be obtained when it is excited at its resonance frequency. Frequency matching is therefore very crucial for every PEH since only 2% deviation of resonance frequency from excitation frequency will drop the electrical output power by 50%. Moreover, the available excitation frequency in real applications is generally between 10 to 30 Hz, which is below the normal resonance frequency of the PEHs. The classical and conventional method to match the resonance frequency with the low excitation frequency is to attach a lumped mass at the tip of the cantilever PEH [38].

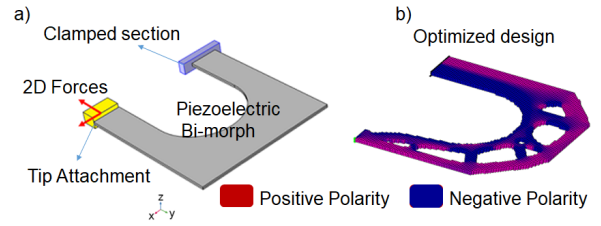


Fig. 5 a) New configuration for frequency tuned piezoelectric energy harvester. b) Topology optimized design [37].

In our recently published work [37], we combined topology optimization and frequency tuning technique to raise further the efficiency of PEH. The idea consists to define a constraint on the fundamental frequency of PEH. To tackle the challenges of eigenfrequency tuning within the topology optimization approach, we defined the attachment's mass as a new optimization variable in addition to the density and polarity. This will be discussed in the next section.

4.4.1 Modeling & Problem formulation

The resonance frequency is the natural frequency of the system at short circuit condition. At open circuit condition, the natural frequencies of the system are the anti-resonance frequency [18]. Therefore the fundamental resonance frequency at $V_p = 0$ can be calculated,

$$\left[\tilde{K}_{uu} - \tilde{M}\tilde{\omega}_s^2 \right] \Psi_s = 0 \quad (25)$$

in which $\tilde{\omega}_s$ is the natural frequency at short circuit condition and Ψ_s is the related eigenvector. Now, based on the built FEM of the piezoelectric plate and the provided resonance equation, topology optimization algorithm can be applied to maximize the harvested energy of the bi-morph vPEH by optimizing the topology and modifying the resonance frequency.

To define the mass of attachment as an optimization variable, we define the mass matrix of the system as follows,

$$\tilde{M} = \sum_{i=1}^{NE} \tilde{m}_i + y[\tilde{M}_{mass}] \quad (0 \leq y \leq 1) \quad (26)$$

Table 2 Summary of publications regarding topology optimization of piezoelectric structures in AS2M department

Year	Publication	Structure	Approach	Contribution
2017	[2]	Uni-morph PEH	Parametric/gradient-based optimization	Explicit cost function to find optimal thickness
2018	[35]	Amplification mechanism	SIMP approach	Increasing the stroke of stack piezo actuator
2020	[29]	single-layer PEH	SIMP approach	Optimization of polarization and topology
2020	[30]	Bi-morph PEH	SIMP approach	Multidirectional PEH/avoiding charge cancelation
2020	[13]	single-layer piezo	SIMP approach	First MATLAB code published for TOM of piezo
2020	[16]	single-layer piezo pusher	SIMP approach	Increasing stroke by optimizing the polarization
2020	[31]	cantilever PEH	Neural network & genetic algorithm	In-span attachment mass
2022	[36]	single-layer piezo pusher	SIMP approach	Considering voltage uncertainty
2023	[37]	Bi-morph PEH	SIMP approach	Tuning resonance frequency/mass optimization

in which \tilde{m}_i is the elemental mass, i is the element number and y is the optimization variable that stands for the ratio of maximum possible mass of the attachment. By definition of y here, we give more freedom to the optimization in terms of convergence to a perfect solid void material in the final layout. The reason is that the variable y can increase or decrease the total mass of the vPEH without changing its stiffness. This optimization variable helps optimization solver to converge to a fully black and white final layout and to avoid the greyness problem which is a common problem in topology optimization with frequency tuning [39].

For tuning the resonance frequency, the first interpolation function defined in equation (9) for the stiffness matrix K_{uu} should be modified to avoid the localized modes at the low density regions [40]. The reason is that, based on the SIMP material interpolation scheme, low density regions are highly flexible (soft) that produce very low and artificial eigenmodes. To remedy, the interpolation function for the stiffness matrix which is proposed by Huang et al. [39] is utilized as follows

$$\tilde{k}_{uu}(x_i) = \left[\frac{x_{min} - x_{min}^{p_{uu}}}{1 - x_{min}^{p_{uu}}} (1 - x_i^{p_{uu}}) + x_i^{p_{uu}} \right] \tilde{k}_{uu} \quad (27)$$

Now, to tune the resonance frequency we modify the problem formulation as follows,

$$\begin{aligned} & \text{minimize } J_{EH} = w_j \Pi^S - (1 - w_j) \Pi^E \\ & \text{Subject to } \quad V(x) = \sum_{i=1}^{NE} x_i v_i \leq V \\ & \quad \quad \quad \omega_1 < \varpi, \\ & \quad \quad \quad 0 \leq x_i \leq 1, \quad 0 \leq P_i \leq 1, \\ & \quad \quad \quad 0 \leq y \leq 1 \end{aligned} \quad (28)$$

where y is the new optimization variable and ϖ is the desired resonance frequency. By having the inequality constraint on the resonance frequency, the optimization is more relaxed than having equality constrained. On the other hand, the resonance frequency will finally match the excitation frequency as the structure tends to be more rigid during optimization iterations. To solve the optimization problem with gradient based optimizers like MMA we need to calculate the sensitivity analysis which will be discussed next.

4.4.2 Sensitivity analysis

Since, the objective function in (28) is the same as (16), we just calculate here the sensitivity of objective function with respect to the new optimization variable as follows

$$\begin{aligned} \frac{\partial \Pi^S}{\partial y} &= \left(\frac{1}{2} \tilde{u}_i^T + \lambda_{1,i}^T \right) \frac{\partial (\tilde{M} \tilde{\Omega}^2)}{\partial y} \tilde{u}_i \\ \frac{\partial \Pi^E}{\partial y} &= \lambda_{2,i}^T \frac{\partial (\tilde{M} \tilde{\Omega}^2)}{y} u_i \end{aligned} \quad (29)$$

where μ and λ are the same elemental adjoint vectors which are calculated in the adjoint equations (20).

To apply the constraint on the natural frequency, its gradient with respect to the optimization variables should be calculated. To do so, the fundamental natural frequency of the system can be defined through the Rayleigh quotient [39],

$$\tilde{\omega}_s^2 = \frac{\Psi_s^T \tilde{K}_{uu} \Psi_s}{\Psi_s^T \tilde{M} \Psi_s} \quad (30)$$

The interpretation of first natural frequency by Rayleigh quotient will result in to more efficient sensitivity analysis. By following the procedure

562 presented in [39], the sensitivities of the natural
 563 frequency's constraints with respect to optimiza-
 564 tion variables are

565

566

567

568

569

570

571

572

$$\begin{aligned} \frac{\partial \omega_s}{\partial x_i} &= \frac{1}{2\omega_s \Psi_s^T \tilde{M} \Psi_s} \left[\Psi_s^T \left(\frac{\partial \tilde{k}_{uu}}{\partial x_i} - \tilde{\omega}_s^2 \frac{\partial \tilde{M}}{\partial x_i} \right) \Psi_s \right] \\ \frac{\partial \omega_s}{\partial y} &= -\frac{\tilde{\omega}_s}{2\Psi_s^T \tilde{M} \Psi_s} \left[\Psi_s^T \frac{\partial \tilde{M}}{\partial y} \Psi_s \right] \end{aligned} \quad (31)$$

573

574

575

576

577

578

579

Now all the required sensitivities are calcu-
 lated. However, since we modified the interpola-
 tion function of the stiffness matrix in equation
 (27) and the expression for the mass matrix is also
 changed, their derivatives with respect to density
 and new mass optimization variable (y) can be
 calculated as:

580

581

582

583

584

585

586

$$\begin{aligned} \frac{\partial \tilde{k}_{uu}}{\partial x} &= \frac{1 - x_{min}}{1 - x_{min}^p} \rho_{uu} x_i^{p-1} K_{uu} \\ \frac{\partial \tilde{m}}{\partial x_i} &= \tilde{m}_i, \quad \frac{\partial \tilde{m}}{\partial y} = \tilde{M}_{mass} \end{aligned} \quad (32)$$

587

588

589

590

591

592

593

594

595

596

Aiming for low weight piezoelectric energy har-
 vester, a new configuration is proposed (Fig. 5-(a))
 to minimize the fundamental resonance frequency
 and the mass of the attachment simultaneously.
 The obtained result (Fig. 5-(b)) in MATLAB and
 COMSOL Multiphysics demonstrated that the
 algorithm successfully restricted the fundamental
 frequency close to the desired one while respecting
 the mass and volume constraints of the vPEH.

597

598

599

600

601

602

603

604

605

606

Simulation results prove the superiority of the
 optimized design in Fig. 5-(b) in comparison with
 the previously optimized design of Fig. 4-(g) while
 having less amount of attachment mass. This is an
 interesting achievement that we restricted the first
 resonance frequency while at the same time having
 a lower amount of weight. On the other hand, the
 stress analysis reveals a higher amount of stress in
 the newly proposed configuration (Fig. 5-(a)) in
 comparison with the previous configuration of the
 PEH (Fig. 5-(g)).

607

608

609

610

611

612

5 MATLAB code for frequency tuning of PEH with mass optimization

In this section the goal is to provide a MAT-
 LAB code for topology optimization of PEH with
 tuning the resonance frequency and considering
 the attached mass as an optimization variable.
 The study of this section is similar to section 4.4.
 However, the dimension of study here is 2D and
 the provided MATLAB code is in 2D as well. It
 should be noted that, despite the modeling dimen-
 sion of the system, the analytical calculations of
 section 4.4 remain true.

The MATLAB code in this section is devel-
 oped on the basis of the previously published
 code from the authors for topology optimization
 of the PEH [13]. Moreover, the case study of this
 section is similar to the case study of the pub-
 lished codes [13] with the difference of considering
 attached mass at the tip of the beam as it has
 been illustrated in Fig. 6 with mass of attach-
 ment as optimization variable. In this case study,
 the polarization direction is considered to be in the z
 direction of the coordinate system. However, it is
 possible to simply consider the polarization direc-
 tion in the y axis and optimize the structure in
 the direction of thickness.

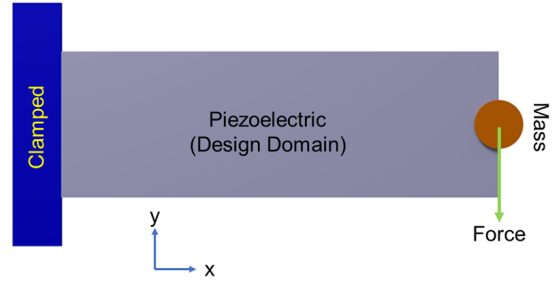


Fig. 6 a) Piezoelectric energy harvester with tip attachment. The mass of attachment is considered as optimization variable.

5.1 Description of the code

The implementation topology optimization MAT-
 LAB code for case study of Fig. 6 is provided in
 the appendix. For the sake of brevity, we will only
 explain here the lines of the code that are different
 from previously published code [13] to implement
 the optimization of resonance frequency. Read-
 ers are advised to read the paper of previously

published codes [13] primarily before reading this section.

5.1.1 Definition of parameters

The provided code starts with the section of GENERAL DEFINITIONS in which the user defines the geometry of the structure, resolution of the mesh, penalty factors, etc. The variable `ft` defines the filtering type in which the user can choose between two filtering methods including density filter [21, 41] or Heaviside projection suggested by Wang et al. [42]. The complete MATLAB implementation code for this combination of filtering methods is provided by Ferrari et al. [43] and the same lines of codes are utilized in the provided code of this paper. Three parameters in the filtering part should be defined in the first section of the code known as filter radius (`rmin`), threshold (`eta`) and sharpness factor (`beta`). The projection filter is new in this code in comparison to previously published codes and it is more efficient in terms of avoiding the gray elements.

For a better convergence to a clean black and white result, the continuation schemes are applied to the penalties and sharpness factor. To do so, `penalCnt`, `betaCnt` are defined similarly to what has been defined by [43]. These parameters accept four values as [`istart`, `maxPar`, `isteps`, `deltaPar`], which means the continuation starts at iteration = `istart` and will be increased by `deltaPar` in each `isteps` and reaching to maximum value `maxPar`.

Variable `DF` determines the maximum desired natural frequency and the Variable `MASS` determines the maximum allowable attachment mass. These two new variables are defined to integrate the frequency tuning and the optimization of attachment mass.

The sections of MATERIAL PROPERTIES, PREPARE FINITE ELEMENT ANALYSIS, DEFINITION OF BOUNDARY CONDITION, FORCE DEFINITION remain intact in comparison to previously published code [13]. Hence, no descriptions will be given here.

The section of DEFINITION OF ATTACHMENT MASS is new and it is defined to model an attachment mass at the tip of the beam. It should be noted that the code is dynamic and the placement of the mass can be changed easily. The lines of code to model the attached mass are as follows:

```

86 %% DEFINITION OF ATTACHMENT MASS
87 sMass=zeros(nele,1);
88 sMass (nele-nely/2) = 1;
89 le = Lp/nely; we = Wp/nely;
90 ro_M = MASS*1e-3/(le*we*h)/length(
      find(sMass));
91 sMMass = (ro_M/ro)*m(:).*sMass';
92 sMMass = reshape(sMMass,length(m(:))
      *nele,1);
93 M_Att = sparse(iK(:),jK(:),sMMass(:)
      ); % Creating mass matrix for
      the attachment mass

```

The method to define the mass is to consider elements at the desired location in the design domain to be more heavy than other elements. To do so, we use the `sMass` which is a Boolean vector with a size of total number of elements. We choose the desired element(s) to place the mass and the rows indexing that element will have the value of 1. In the case study of this paper, since we placed the mass of attachment at the end of the beam as illustrated in Fig. 6, the last element at the tip of the beam in the middle of the width is chosen to be heavier than the rest of the element. To make the element heavier, we modify the density of the elemental mass matrix by `ro_M`. Finally, this mass will be augmented to the global size mass matrix with the help of the `sMMass`. The `M_Att` is a matrix with the size of global mass matrix which only contains the attached mass. As such, it should be augmented to global piezoelectric mass matrix which will be explained later.

The section of PREPARE FILTER is transferred from the code written by Ferrari. et. al [43] to implement the density filter and projection. A detailed explanation can be found in the cited reference. In the section of INITIALIZE ITERATION we defined the ratios for the continuation scheme. These ratios guarantee that the necessary conditions between the penalization factors of piezoelectric matrices will follow the intrinsic conditions suggested by [44] during the continuation scheme of penalization factors. `NATD` is the normalized desired natural frequency. `Ym` is the optimization variable for the attachment mass that it has set to zero as the initial value before the optimization.

In the section of MMA Preparation, we set the initial values for the the MMA optimizer. However, the MMA code will not be presented in the

613
614
615
616
617
618
619
620
621
622
623
624
625
626
627
628
629
630
631
632
633
634
635
636
637
638
639
640
641
642
643
644
645
646
647
648
649
650
651
652
653
654
655
656
657
658
659
660
661
662
663

664 paper and these are external codes that are called
665 in our code. To have the MMA code, a request by
666 reader should be sent to the author of the MMA
667 paper [25, 26].

668 5.1.2 Iteration loop

670 In the section of START ITERATION, we start
671 the optimization iterations. Iteration loop start
672 by the filter/projection part which is again trans-
673 ferred from the code written by Ferrari et al. [43].
674 This initial part of iteration loop produce the
675 projected physical densities (xPhys).

676 The interpolation function mentioned in
677 equation (27), is implemented in following line:
678

```
679 146 xPhysH = ((xpmín-xpmín.^penalKuu
680 ) ./ (ones(nely,nelx)-xpmín.^
681 penalKuu)) .* (ones(nely,nelx)-
682 xPhys.^penalKuu)+xPhys.^penalKuu
683 ; % kuu interpolation function
```

684 The line after, produces the derivation of
685 (xPhysH) with respect to (xPhys) which is nec-
686 essary for the sensitivity analysis:
687

```
688 147 xPhysHD = penalKuu*((ones(nely,
689 nelx)-xpmín) ./ (ones(nely,nelx)-
690 xpmín.^penalKuu)) .* xPhys.^(
691 penalKuu-1); % Derivation of
692 xPhysH with respect to xPhys
```

693 In the part of (FE-ANALYSIS), the column
694 vectors sM, sKuu, sKup, sKpp will be used
695 to create the mass matrix, stiffness matrix, cou-
696 pling matrix and permittivity matrix respectively
697 all at the global (system) level.

698 In the following line, the attachment mass
699 multiplied to optimization variable (Ym), will be
700 augmented to the global mass matrix:
701

```
702 155 Mtot = M + M_Att*Ym; %
703 Augmenting attached mass
```

704 The natural frequency and the related eigen-
705 vector of the system are calculated in the following
706 line:
707

```
708 157 [EIGVs, NATs]=eigs(Kuu(freedofs,
709 freedofs), Mtot(freedofs, freedofs)
710 ), 1, 'smallestabs'); Freq=sqrt(
711 NATs*k0/M0)/(2*pi); %
712 Calculation of natural frequency
```

The variable Freq produces the real natural
frequency in Hertz by rolling back the normaliza-
tion. In next line, eigenvector is normalized with
respect to mass matrix:

```
158 Normal=EIGVs'*M(freedofs,
freedofs)*EIGVs; EIGV(freedofs)=
sqrt(1/(Normal(1,1)))*EIGVs; %
Normalization of eigenvector
```

The constitution of global matrices and solv-
ing the finite element equilibrium equation and
adjoint equations remain the same as previous
code [13]. In the part of OBJECTIVE FUNCTION
AND SENSITIVITY ANALYSIS, the mechanical
energy is divided to two parts related to k_{uu} and
 $-m\Omega^2$.

The sensitivity of objective function related
the attachment mass which has been mentioned in
equation (29), is calculated in the following line:

```
192 dY = dY + (ro_M/ro)*(1/(
length(find(sMass))))*reshape(
full(sum(dcME.*sMass,2)), [nelx,
nely]); dY = sum(dY(:)); %
Attachement sensitivity
```

The sensitivities of natural frequency with
respect to density and mass ratio (y) which are
mentioned in equation (31) are calculated in fol-
lowing lines:

```
194 DCKE=(1/(2*sqrt(NATs)))*((1/2)*
EIGV(edofMat)*kku) .* EIGV(edofMat
)); DCK = reshape(sum(DCKE,2), [
nely,nelx]);
195 DCME=(1/(2*sqrt(NATs)))*((1/2)*
EIGV(edofMat)*(-m*NATs)) .* EIGV(
edofMat); DCM = reshape(sum(DCME
,2), [nely,nelx]);
196 dcF=(E0-Emin)*xPhysHD.*DCK+DCM;
% Frequency sensitivity (density
)
197 DcF_Y = (ro_M/ro)*(1/(length(
find(sMass))))*reshape(sum(full(
DCME.*sMass),2), [nely,nelx]);
DcF_Y = sum(DcF_Y(:)); %
Frequency sensitivity (
attachement mass)
```

All the calculated sensitivities are filtered
using the MATLAB built-in function imfilter
as suggested by Ferrari et al. [43].

The section of MMA OPTIMIZATION OF
DESIGN VARIABLES calls MMA optimizer to

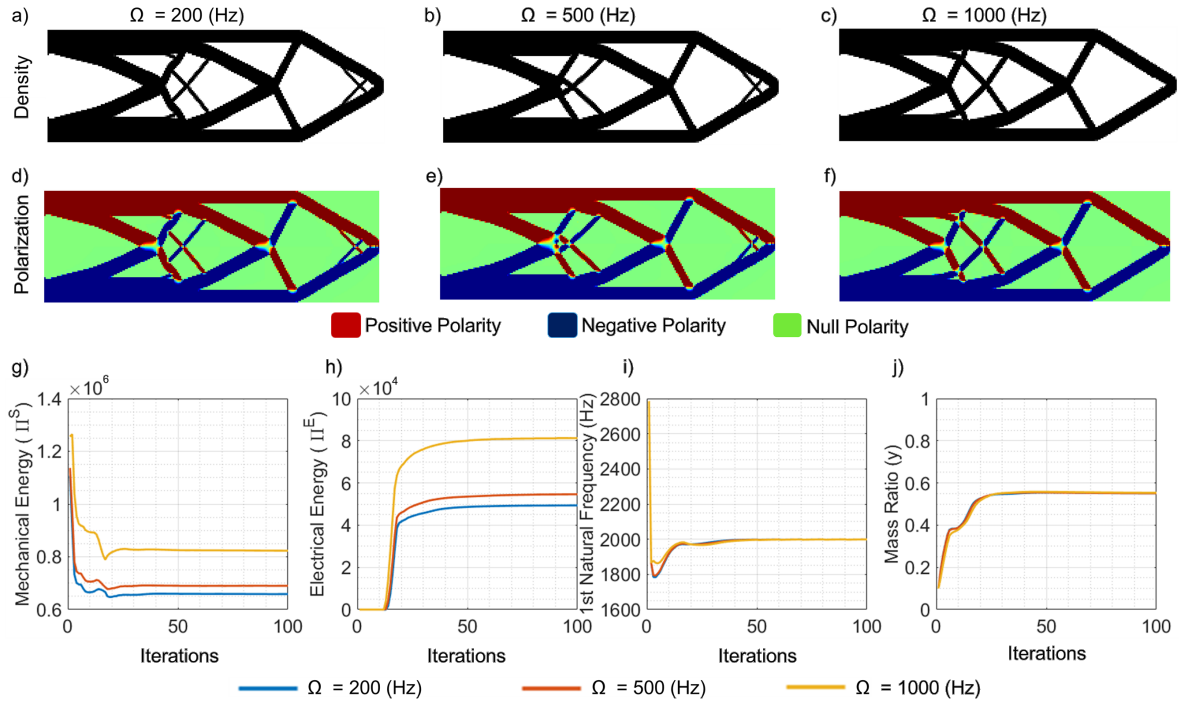


Fig. 7 Topology optimization result for PEH energy harvester for different excitation frequency. Desired natural frequency = 2000 (Hz). a-c) Layout results, d-f) Polarization profile, g-j) Numerical plots.

update the optimization variables. The external codes which are called in this section are `mmasub.m` and `subsolve.m` which should be requested from the author of the papers [25, 26].

After updating the optimization variables, the continuation scheme will be applied to the penalization factor and sharpness factor for the next iteration. The engagement of this continuation scheme will be done in a particular iteration number defined by the user as explained before.

5.1.3 Presentation of results

The final section of the paper is `PLOT DENSITIES & POLARIZATION` which show the density and polarization profile in each iteration plus showing the numerical results.

5.2 Case studies

To analyze the efficiency of the code, three case studies are investigated. For all of the case studies the optimization problem is formulated as it is mentioned in equation (28) which means the structure in Fig. 6 is under harmonic excitation and while there is a constraint on the fundamental (first) natural frequency, the goal is to maximize the output electrical energy VS mechanical

energy. The optimization variables are the density, polarization and attachment's mass.

5.2.1 Various excitation frequency, Constant constraint on the natural frequency

In the first case study, the structure will be excited by three different frequencies while the constraint on the natural frequency is equivalent to 2000 Hz. The results of optimization are illustrated in Fig. 7. As it can be seen in this figure, different optimal layouts are obtained for different excitation frequencies. This was also studied in the previously published code [13]. However, the important points here can be seen in the numerical results. In panel (i) of Fig. 7 it is obvious that in all cases the optimization respected the constraint on the natural frequency precisely. The results are quite satisfactory considering the fact that the optimal layouts are completely steered to fully black and white and gray elements are successfully avoided. Although the filtering and projection were efficient in this case, the major factor is the optimization of the attachment's mass. As can be seen in panel (j),

715
716
717
718
719
720
721
722
723
724
725
726
727
728
729
730
731
732
733
734
735
736
737
738
739
740
741
742
743
744
745
746
747
748
749
750
751
752
753
754
755
756
757
758
759
760
761
762
763
764
765

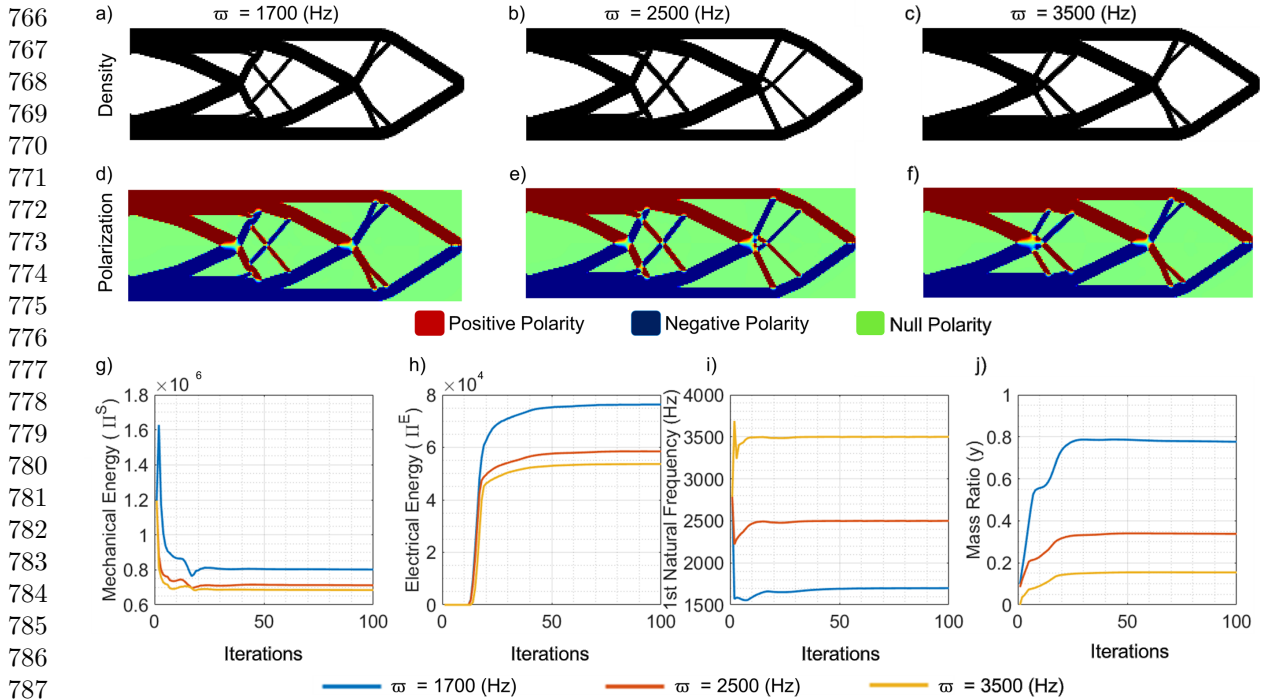


Fig. 8 Topology optimization result for PEH energy harvester for different desired natural frequency. Excitation frequency = 800 (Hz). a-c) Layout results, d-f) Polarization profile, g-j) Numerical plots.

the optimization variable (y) gradually increased during the optimization to reduce the overall natural frequency of the system. This gives more freedom to the optimization solver to increase the mass of the structure without modifying its stiffness.

5.2.2 Constant excitation frequency, different constraint on the natural frequency

In the next case study, the results of optimization for different constraints on the natural frequency are reported in Fig. 8. In panels (i) and (j) of this figure, it can be seen that the constraint on the natural frequency is respected with different final attachment mass. When the constraint on the natural frequency is very low, higher mass is required to decrease the natural frequency and vice versa.

5.2.3 Different maximum allowable attachment's mass

In the final case study, the results of optimization for different maximum allowable attachment's mass are illustrated in Fig. 9. In this case study,

a constant constraint on the natural frequency and a constant excitation frequency are considered for three different attachment's mass. Moreover, the final optimal attachment's mass (mass ratio times the maximum allowable mass) is the same. However, still, the optimal layouts (panels (a-c)), are different. This can be due to the fact that the maximum allowable jump between the values of optimization variables in two sequences of iteration is limited. Hence, the design with more allowable mass respects the constraint sooner.

The provided MATLAB code in this section can be extended to 3D problem. In this regard, the strategy and structure of the code remains the same. The provided MATLAB code is flexible in terms of considering different case studies i.e. different boundary conditions and force applications, design domain, etc.

6 Toward multi-material topology optimization

In pursuit of advancing the application of topology optimization to piezoelectric structures, AS2M

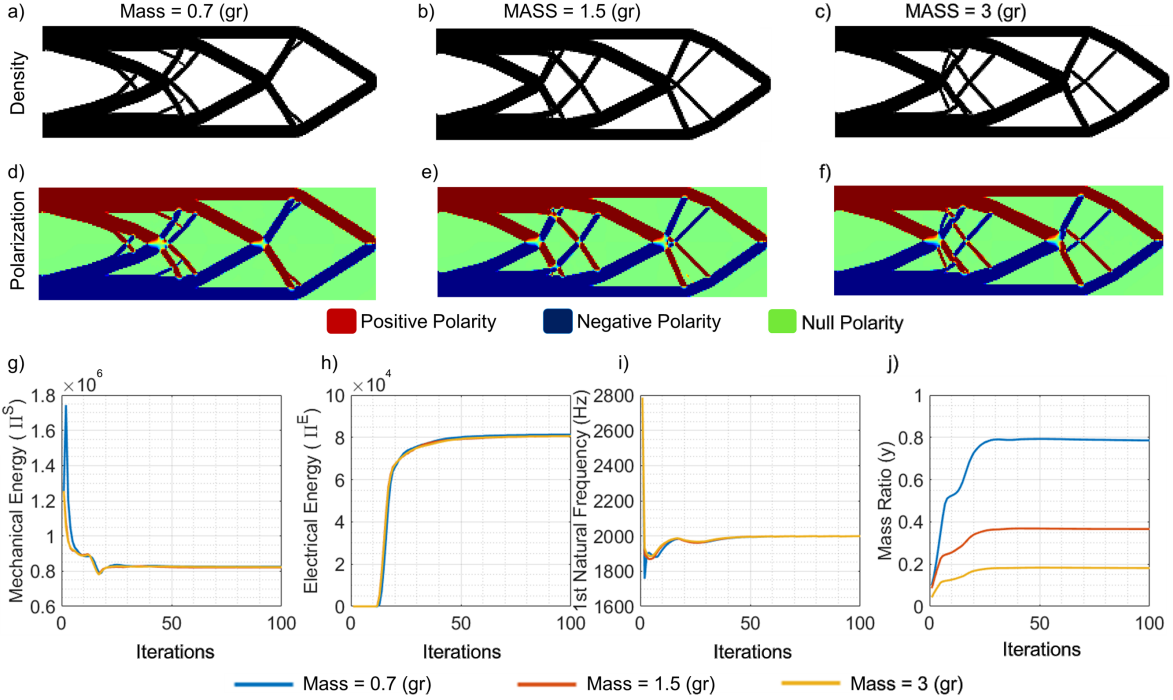


Fig. 9 Topology optimization result for PEH energy harvester for different attached mass. Excitation frequency = 800 (Hz) and desired natural frequency = 2000 (Hz). a-c) Layout results, d-f) Polarization profile, g-j) Numerical plots.

department embarked on a new initiative. Building upon the proven success of topology optimization using single material, particularly in the design of piezoelectric energy harvesters (PEHs) and piezoelectric actuators as summarized in Table 2, this new venture seeks to simultaneously distribute both active and passive materials.

The research on multi-material has reached a mature stage, as evidenced by several notable works [45–48]. Multi-material topology optimization (MMTO) involves the integration of soft materials and passive materials, drawing inspiration from natural systems. This innovative design methodology strives to achieve an optimal equilibrium between the flexibility inherent in soft piezoelectric materials and the sturdiness of rigid passive materials.

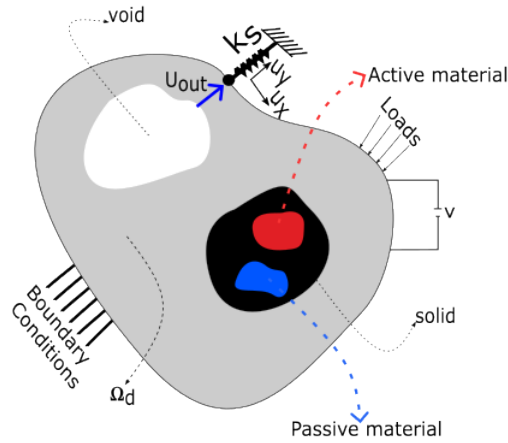
Leveraging multi-material topology optimization provides an avenue to fully exploit the inherent advantages of using different materials to enhance structural performance. This approach leads to an increase in the degrees of freedom in force, displacement and energy transduction particularly in the context of piezoelectric materials [49]. The process of incorporating multi-material

technique into the design of robotic structures as given in the design of Robobee, MiGriBot and MilliDelta involves the optimal combination of two distinct materials to leverage their individual inherent characteristics through a unified approach. This integration is crucial for optimizing the overall performance of the robotic systems.

A key technique employed in this endeavor is topology optimization (TO) particularly utilizing the well established Solid Isotropic Materials with Penalization (SIMP) method. The literature primarily addresses cases of combination of multi-material such as passive-passive, active-active and active-passive materials.

The multi-material scheme is responsible for creation of a design domain comprising of three phases: void and two solid phases corresponding to either void or passive materials as depicted in Fig. 10.

817
818
819
820
821
822
823
824
825
826
827
828
829
830
831
832
833
834
835
836
837
838
839
840
841
842
843
844
845
846
847
848
849
850
851
852
853
854
855
856
857
858
859
860
861
862
863
864
865
866
867



882 **Fig. 10** Piezoelectric multi-material actuator design
 883 domain with loading and boundary conditions

886 7 Conclusion

887 This paper primarily summarized and discussed
 888 the approaches developed at AS2M/FEMTO-ST
 889 institute for the topological design of piezoelectric
 890 structures. The summary of the publications and
 891 the introduced contribution is reported in Table
 892 2. We demonstrated that topology optimization
 893 methodology can be employed as a design tool to
 894 obtain miniaturized piezoelectric structures with
 895 enhanced performances. Moreover, the eigenvalue
 896 and mass optimization of the PEH are presented
 897 in the paper theoretically and a 2D topology opti-
 898 mization MATLAB code is provided to tune the
 899 frequency of a piezoelectric energy harvester by
 900 optimizing the mass of the attachment. This is a
 901 first and new code in the literature in this context.
 902

903 Extending the SIMP to piezoelectric material
 904 paves the way for promising perspectives. The first
 905 perspective would concern multi-material topol-
 906 ogy optimization including active and passive
 907 material. The other perspectives would concern
 908 multi-degrees of freedom structures and consider-
 909 ation of large deformations.

910 **Supplementary information.** This paper is
 911 accompanied by MATLAB codes with format
 912 of .m file. The code is uploaded a supple-
 913 mentary material of this paper which can
 914 be downloaded from the journal publication
 915 page or from the GitHub of the author:
 916 <https://github.com/AbbasHomayouni> .
 917

Acknowledgments. This work was supported
 by MultiOptim Chrysalide emergent project
 (UFC) and the Conseil Regional de Bourgogne
 Franche-Comte (France) Robocap project. It was
 also partially supported by the national CODE-
 TRACK project (ANR-17-CE05-0014-01), the
 Conseil Regional de Bourgogne Franche-Comté
 CONAFLU project and ANR OptoBot project.

MATLAB TOPOLOGY OPTIMIZATION CODE FOR PIEZOELECTRIC ENERGY HARVESTERS WITH FREQUENCY TUNING

```

1 % A 2D TOPOLOGY OPTIMIZATION CODE FOR PIEZOELECTRIC ENERGY HARVESTER WITH
  FREQUENCY TUNING
2 clc;clear;close all;
3 %% GENERAL DEFINITIONS
4 Lp = 3e-2; % Piezoelectric plate length (m) in x direction
5 Wp = 1e-2; % Piezoelectric plate width (m) in y direction
6 h = 2e-4; % Piezoelectric plate Thickness (m) in z direction
7 nelx = 240; % Number of element in x direction
8 nely = 80; % Number of element in y direction
9 penalKuu = 3; penalKup = 6;penalKpp = 4;penalPol = 1; % Penalization factors
10 omega = 800; % Excitation frequency (Hz)
11 wj = 0.2; % Objective function weigthing factor
12 volfrac = 0.5; % Volume fraction
13 ft = 2; % l= Density filter, 2&3= projection with eta and beta as parameters
14 rmin = 2; % Filter radius
15 eta = 0.5; % Threshold
16 beta = 1; % Sharpness factor
17 ftBC = 'N';
18 penalCnt = {50,6,10,0.1}; % Continuation scheme on penalKuu {istart, maxPar,
  isteps, deltaPar}
19 betaCnt = {50,60,10,1}; % Continuation scheme on beta {istart, maxPar, isteps,
  deltaPar}
20 DF = 2000; % Desired fundamental natural frequency (Hz)
21 MASS = 1; % Maximum allowable attachment mass (gr)
22 Max_loop = 100; % Maximum number of Iterations
23 %% MATERIAL PROPERTIES (PZT 4)
24 ro = 7500; % Density of piezoelectric material
25 e31 = -14.9091; % e31 Coupling coefficient
26 ep33 = 7.8374e-09; % Piezoelectric permitivity epsilon33
27 C = zeros(3,3); % Creation of null mechanical stiffness tensor
28 C(1,1) = 9.1187e+10; C(2,2) = C(1,1);
29 C(1,2) = 3.0025e+10; C(2,1) = C(1,2);
30 C(3,3) = 3.0581e+10;
31 %% PREPARE FINITE ELEMENT ANALYSIS
32 le = Lp/nelx; % Element length
33 we = Wp/nely; % Element width
34 e = [e31,e31,0]; % Piezoelectric matrix
35 x1 = 0;y1 = 0;x2 = le;y2 = 0;x3 = le;y3 = we;x4 = 0;y4 = we; % Element node
  coordinate
36 GP = [-1/sqrt(3) -1/sqrt(3);1/sqrt(3) -1/sqrt(3);1/sqrt(3) 1/sqrt(3);-1/sqrt(3)
  1/sqrt(3)]; % Gauss quadrature points
37 kuu = 0;kpp = 0;kup = 0;m = 0; % Initial values for piezoelectric matrices
38 for i = 1:4
39     s = GP(i,1);t = GP(i,2); % Natural coordinates
40     n1 = (1/4)*(1-s)*(1-t);
41     n2 = (1/4)*(1+s)*(1-t);
42     n3 = (1/4)*(1+s)*(1+t);
43     n4 = (1/4)*(1-s)*(1+t);
44     a = (y1*(s-1)+y2*(-1-s)+y3*(1+s)+y4*(1-s))/4;
45     b = (y1*(t-1)+y2*(1-t)+y3*(1+t)+y4*(-1-t))/4;
46     c = (x1*(t-1)+x2*(1-t)+x3*(1+t)+x4*(-1-t))/4;
47     d = (x1*(s-1)+x2*(-1-s)+x3*(1+s)+x4*(1-s))/4;

```

919
920
921
922
923
924
925
926
927
928
929
930
931
932
933
934
935
936
937
938
939
940
941
942
943
944
945
946
947
948
949
950
951
952
953
954
955
956
957
958
959
960
961
962
963
964
965
966
967
968
969

```

970 48 B1 = [a*(t-1)/4-b*(s-1)/4 0 ; 0 c*(s-1)/4-d*(t-1)/4 ;c*(s-1)/4-d*(t-1)/4 a*(
971 t-1)/4-b*(s-1)/4];
972 49 B2 = [a*(1-t)/4-b*(-1-s)/4 0 ; 0 c*(-1-s)/4-d*(1-t)/4;c*(-1-s)/4-d*(1-t)/4 a
973 *(1-t)/4-b*(-1-s)/4];
974 50 B3 = [a*(t+1)/4-b*(s+1)/4 0 ; 0 c*(s+1)/4-d*(t+1)/4 ;c*(s+1)/4-d*(t+1)/4 a*(
975 t+1)/4-b*(s+1)/4];
976 51 B4 = [a*(-1-t)/4-b*(1-s)/4 0 ; 0 c*(1-s)/4-d*(-1-t)/4 ;c*(1-s)/4-d*(-1-t)/4
977 a*(-1-t)/4-b*(1-s)/4];
978 52 Bfirst = [B1 B2 B3 B4];
979 53 Jfirst = [0 1-t t-s s-1 ; t-1 0 s+1 -s-t ;s-t -s-1 0 t+1 ; 1-s s+t -t-1 0];
980 54 J = [x1 x2 x3 x4]*Jfirst*[y1 ; y2 ; y3 ; y4]/8; % Determinant of jacobian
981 matrix
982 55 Bu = Bfirst/J;
983 56 Bphi = 1/h;
984 57 kuu = kuu + h*J*transpose(Bu)*C*Bu; % Mechanical stiffness matrix
985 58 kup = kup + h*J*transpose(Bu)*e'*Bphi; % Piezoelectric coupling matrix
986 59 kpp = kpp + h*J*transpose(Bphi)*ep33*Bphi; % Dielectric stiffness matrix
987 60 N = [n1, 0, n2, 0, n3, 0, n4, 0; 0, n1, 0, n2, 0, n3, 0, n4]; % Matrix of interpolation
988 functions
989 61 m = m+J*ro*h*(N')*N; % Mass matrix
990 62 end
991 63 k0 = max(abs(kuu(:)));beta0 = max(kpp(:));alpha = max(kup(:));M0 = max(m(:)); %
992 Normalization Factors
993 64 kuu = kuu/k0;kup = kup/alpha;kpp = kpp/beta0;gamma = (k0*beta0)/(alpha^2);m = m/
994 M0; omega = M0*(omega*2*pi)^2/k0; % Normalization
995 65 ndof = 2*(nely+1)*(nelx+1); % mechanical degrees of freedom
996 66 nele = nelx*nely; % number of elements
997 67 nodenrs = reshape(1:(1+nelx)*(1+nely),1+nely,1+nelx);
998 68 edofVec = reshape(2*nodenrs(1:end-1,1:end-1)+1,nele,1);
999 69 edofMat = repmat(edofVec,1,8)+repmat([0 1 2*nely+[2 3 0 1] -2 -1],nele,1);
1000 70 edofMatPZT = 1:nele;
1001 71 iK = kron(edofMat,ones(8,1))';
1002 72 jK = kron(edofMat,ones(1,8))';
1003 73 iKup = edofMat';
1004 74 jKup = kron(edofMatPZT,ones(1,8))';
1005 75 B = ones(nele,1); % Boolean Matrix defined as a vector of ones
1006 76 %% DEFINITION OF BOUNDARY CONDITION
1007 77 fixeddofs = 1:2*(nely+1); % Clamped-Free
1008 78 freedofs = setdiff(1:ndof,fixeddofs);
1009 79 lf = length(freedofs);
1010 80 %% FORCE DEFINITION
1011 81 nf = 1; % Number of forces
1012 82 F = sparse(ndof,nf);
1013 83 Fe = ndof-(nely); % Definition of desired Dof for application of force
1014 84 F(Fe,1) = +1; % Amplitude of the force
1015 85 Ftot = [F(freedofs,:);zeros(1,nf)];
1016 86 %% DEFINITION OF ATTACHMENT MASS
1017 87 sMass=zeros(nele,1);
1018 88 sMass (nele-nely/2) = 1;
1019 89 le = Lp/nelx; we = Wp/nely;
1020 90 ro_M = MASS*1e-3/(le*we*h)/length(find(sMass));
1021 91 sMMass = (ro_M/ro)*m(:).*sMass';
1022 92 sMMass = reshape(sMMass,length(m(:))*nele,1);
1023 93 M_Att = sparse(iK(:),jK(:),sMMass(:)); % Creating mass matrix for the
1024 attachment mass

```

```

94 %% PREPARE FILTER (F. Ferrari et al. 2021) 1021
95 if ftBC == 'N', bcF = 'symmetric'; else, bcF = 0; end 1022
96 prj = @(v, eta, beta) (tanh(beta*eta)+tanh(beta*(v(:)-eta)))/(tanh(beta*eta)+tanh 1023
    (beta*(1-eta))); % projection 1024
97 deta = @(v, eta, beta) - beta * csch( beta ) .* sech( beta * ( v( : ) - eta ) ).^2 1025
    .*sinh( v( : ) * beta ) .* sinh( ( 1 - v( : ) ) * beta ); % projection eta 1026
    -derivative 1027
98 dprj = @(v, eta, beta) beta*(1-tanh(beta*(v-eta)).^2)/(tanh(beta*eta)+tanh(beta 1028
    *(1-eta))); % proj. x-derivative 1029
99 cnt = @(v, vCnt, l) v+(1>=vCnt{1}).*(v<vCnt{2}).*(mod(l, vCnt{3})==0).*vCnt{4}; 1030
100 [dy, dz, dx] = meshgrid(-ceil(rmin)+1:ceil(rmin)-1, -ceil(rmin)+1:ceil(rmin)-1, - 1031
    ceil(rmin)+1:ceil(rmin)-1 ); 1032
101 h = max( 0, rmin - sqrt( dx.^2 + dy.^2 + dz.^2 ) ); % Conv. kernel 1033
102 Hp = imfilter( ones( nely, nelx), h, bcF ); dHs = Hp; % Matrix of weights ( 1034
    filter) 1035
103 %% INITIALIZE ITERATION 1036
104 x = repmat(volfrac, nely, nelx); xpmin=x*1e-2; % Initial values for density ratios 1037
105 pol = repmat(0.5, [nely, nelx]); % Initial values for polarization 1038
106 xPhys = x; 1039
107 loop = 0; 1040
108 Density_change = 1; 1041
109 E0 = 1; Emin = 1e-9; 1042
110 e0 = 1; eMin = 1e-9; 1043
111 eps0 = 1; epsMin = 1e-9; 1044
112 dv0 = ones(nely, nelx); % Volume sensitivity 1045
113 penalratio_up = penalKup/penalKuu; penalratio_pp = penalKpp/penalKuu; % Penalty 1046
    ratios for continuation scheme 1047
114 NATD=(DF*2*pi)^2*(M0/k0); % Normalization of desired natural frequency 1048
115 Ym = 0; % Initial mass ratio 1049
116 EIGV1 = zeros( ndof, 1); EIGV2 = zeros( ndof, 1); % Creating null eigenvectors 1050
117 %% MMA Preparation 1051
118 mc = 2; % Number of constraints 1052
119 nVar = 2*nele+1; % Number of variables 1053
120 xmin = zeros(nVar, 1); % Minimum possible density 1054
121 xmax = ones(nVar, 1); % Vector of maximum optimization variables 1055
122 xold1 = [x(:); pol(:); Ym]; % Vector of variables for previous iteration 1056
123 xold2 = [x(:); pol(:); Ym]; % Vector of variables for 2nd previous iteration 1057
124 low = xmin; % Initial vector of lower asymptotes 1058
125 upp = xmax; % Initial vector of upper asymptotes 1059
126 a0 = 1; 1060
127 ai = zeros(mc, 1); 1061
128 ci = (1e5)*ones(mc, 1); 1062
129 di = zeros(mc, 1); 1063
130 %% START ITERATION 1064
131 while Density_change > 0.005 && loop < Max_loop 1065
132     tic 1066
133     loop = loop + 1; 1067
134     % COMPUTE PHYSICAL DENSITY FIELD (AND ETA IF PROJECT.) (F. Ferrari et al. 1068
    2021) 1069
135     xTilde = imfilter( reshape( x, nely, nelx), h, bcF ) ./ Hp; xPhys = xTilde; 1070
        % Filtered field 1071
136     if ft > 1 % Compute optimal eta* with Newton 1072
137         f = ( mean( prj( xPhys, eta, beta ) ) - volfrac ) * (ft == 3); % 1073
        Function (volume) 1074
138         while abs( f ) > 1e-6 % Newton process for finding opt. eta 1075

```

```

1072 139         eta = eta - f / mean( deta( xPhys, eta, beta ) );
1073 140         f = mean( prj( xPhys, eta, beta ) ) - volfrac;
1074 141     end
1075 142     dHs = Hp ./ reshape( dprj( xPhys, eta, beta ), nely, nelx); %
Sensitivity modification
1076 143     xPhys = prj( xPhys, eta, beta ); % Projected (physical) field
1077 144     end
1078 145     xPhys = reshape(xPhys,nely,nelx); % Physical density
1079 146     xPhysH = ((xpmin-xpmin.^penalKuu)./(ones(nely,nelx)-xpmin.^penalKuu)).*(ones
1080 147     (nely,nelx)-xPhys.^penalKuu)+xPhys.^penalKuu; % kuu interpolation function
1081 147     xPhysHD = penalKuu*(ones(nely,nelx)-xpmin)./(ones(nely,nelx)-xpmin.^
1082 148     penalKuu)).*xPhys.^(penalKuu-1); % Derivation of xPhysH with respect to
1083 149     xPhys
1084 150     % FE-ANALYSIS
1085 151     sM = m(:)*xPhys(:)';
1086 152     sKuu = kuu(:).*(Emin+xPhysH(:)'.*(E0-Emin));
1087 153     sKup = kup(:)*(eMin+xPhys(:)'.^penalKup*(e0-eMin).*((2*pi)-1)'.^penalPol
1088 154     );
1089 155     sKpp = kpp(:)*(epsMin+xPhys(:)'.^penalKpp*(eps0-epsMin));
1090 156     % Creation of global matrices
1091 157     M = sparse(iK(:),jK(:),sM(:)); M = (M+M')/2; % Global mass matrix
1092 158     Mtot = M + MAtt*Ym; % Augmenting attached mass
1093 159     Kuu = sparse(iK,jK,sKuu);
1094 160     [EIGVs,NATs]=eigs(Kuu(freedofs,freedofs),Mtot(freedofs,freedofs),1,'
smallestabs');Freq=sqrt(NATs*k0/M0)/(2*pi); % Calculation of natural
1095 161     frequency
1096 162     Normal=EIGVs'*M(freedofs,freedofs)*EIGVs; EIGV(freedofs)=sqrt(1/(Normal(1,1)
1097 163     ))*EIGVs; % Normalization of eigenvector
1098 164     Kuu = sparse(iK,jK,sKuu)-omega*Mtot;
1099 165     Kup = sparse(iKup(:),jKup(:),sKup(:)); % Global piezoelectric coupling
1100 166     matrix
1101 167     Kpp = sparse(edofMatPZT(:),edofMatPZT(:),sKpp(:)); % Global dielectric
1102 168     stiffness matrix
1103 169     KupEqui = Kup(freedofs,:)*B; KppEqui = gamma*B'*Kpp*B; % Equipotential
1104 170     Condition
1105 171     Ktot = [Kuu(freedofs,freedofs),KupEqui;KupEqui',-KppEqui]; % Creation of
1106 172     total matrix with equipotential hypothesis
1107 173     Ktot = 1/2*(Ktot + Ktot'); % Numerical symmetry enforcement
1108 174     U = Ktot\Ftot; % Response vector
1109 175     Uu(freedofs,:) = U(1:lf,:); Up = U(lf+1:end,:); % Separation of mechanical
1110 176     displacement and electrical Potential
1111 177     ADJ1 = Ktot\[-Kuu(freedofs,freedofs)*Uu(freedofs,);zeros(1,nf)]; % First
1112 178     adjoint vector
1113 179     lambda1(freedofs,:) = ADJ1(1:lf,:); mu1 = B*ADJ1(lf+1:end,:);
1114 180     ADJ2 = Ktot\[zeros(lf,nf);-KppEqui*Up]; % Second adjoint vector
1115 181     lambda2(freedofs,:) = ADJ2(1:lf,:); mu2 = B*ADJ2(lf+1:end,:);
1116 182     % OBJECTIVE FUNCTION AND SENSITIVITY ANALYSIS
1117 183     c = 0; Wm1 = 0; Wm2 = 0; We = 0;
1118 184     dc = zeros(nely,nelx);
1119 185     dp = zeros(nely,nelx);dY = 0;
1120 186     for i = 1:nf % nf is the total number of forces (Load Cases)
1121 187         Uu_i = Uu(:,i);Up_i = B*Up(:,i);
1122 188         lambda1_i = lambda1(:,i); lambda2_i = lambda2(:,i);
1123 189         mu1_i = mu1(:,i); mu2_i = mu2(:,i);

```

```

179     Wm1 = Wm1 + reshape(sum((Uu_i(edofMat)*kku).*Uu_i(edofMat),2),nely,nelx); 1123
    % Elemental mechanical energy (kku) 1124
180     Wm2 = Wm2 + reshape(sum((Uu_i(edofMat)*m*omega).*Uu_i(edofMat),2),nely, 1125
nelx); % Elemental mechanical energy (m) 1126
181     We = We + reshape(sum((Up_i*kpp).*Up_i,2),nely,nelx); % Elemental 1127
electrical energy 1128
182     dcKuuE = wj*(((1/2)*Uu_i(edofMat) + lambda1_i(edofMat))*kku).*Uu_i( 1129
edofMat)-(1-wj)*((lambda2_i(edofMat)*kku).*Uu_i(edofMat)); 1130
183     dcKupE = wj*((lambda1_i(edofMat)*kup).*Up_i + ((Uu_i(edofMat))*kup).* 1131
mul_i)-(1-wj)*((lambda2_i(edofMat)*kup).*Up_i + ((Uu_i(edofMat))*kup).*mu2_i); 1132
184     dcKppE = wj*((-mul_i*kpp).*Up_i)-(1-wj)*((1/2)*(Up_i*kpp).*Up_i - (mu2_i* 1133
kpp).*Up_i); 1134
185     dcME = wj*(((1/2)*Uu_i(edofMat) + lambda1_i(edofMat))*(-m*omega)).*Uu_i( 1135
edofMat)-(1-wj)*((lambda2_i(edofMat))*(-m*omega)).*Uu_i(edofMat)); 1136
186     dcKuu = reshape(sum(dcKuuE,2),[nely,nelx]); 1137
187     dcKup = reshape(sum(dcKupE,2),[nely,nelx]); 1138
188     dcKpp = gamma*reshape(sum(dcKppE,2),[nely,nelx]); 1139
189     dcM = reshape(sum(dcME,2),[nely,nelx]); 1140
190     dc = dc + (E0-Emin)*xPhysHD.*dcKuu+penalKup*(e0-eMin)*xPhys.^(penalKup 1141
-1).*dcKup.*(2*pol-1).^(penalPol)+penalKpp*(eps0-epsMin)*xPhys.^(penalKpp 1142
-1).*dcKpp+dcM; % Density sensitivity 1143
191     dp = dp + (e0-eMin)*2*penalPol*(2*pol-1).^(penalPol-1).*xPhys.^( 1144
penalKup.*dcKup); % Polarization sensitivity 1145
192     dY = dY + (ro_M/ro)*(1/(length(find(sMass))))*reshape(full(sum(dcME.* 1146
sMass,2)),[nelx,nely]);dY = sum(dY(:)); % Attachment sensitivity 1147
193     end 1148
194     DCKE=(1/(2*sqrt(NATs)))*(((1/2)*EIGV(edofMat)*kku).*EIGV(edofMat));DCK = 1149
reshape(sum(DCKE,2),[nely,nelx]); 1150
195     DCME=(1/(2*sqrt(NATs)))*(((1/2)*EIGV(edofMat))*(-m*NATs)).*EIGV(edofMat));DCM 1151
= reshape(sum(DCME,2),[nely,nelx]); 1152
196     dcF=(E0-Emin)*xPhysHD.*DCK+DCM; % Frequency sensitivity (density) 1153
197     DcF_Y = (ro_M/ro)*(1/(length(find(sMass))))*reshape(sum(full(DCME.*sMass),2) 1154
,[nely,nelx]);DcF_Y = sum(DcF_Y(:)); % Frequency sensitivity (attachement 1155
mass) 1156
198     Wm = sum(sum(xPhysH.*Wm1))-sum(sum(xPhys.*Wm2)); % Mechanical energy ( 1157
Normalized) 1158
199     We = sum(sum((epsMin+xPhys.^(penalKpp*(eps0-epsMin))).*We)); % Electrical 1159
energy (Normalized) 1160
200     c = wj*Wm-(1-wj)*We; % Objective function 1161
201     dv = ones(nely,nelx); 1162
202     % FILTERING/MODIFICATION OF SENSITIVITIES 1163
203     dc = imfilter( reshape( dc, nely, nelx) ./ dHs, h, bcF ); % Filter objective 1164
sensitivity 1165
204     dcF = imfilter( reshape( dcF, nely, nelx) ./ dHs, h, bcF ); % Filter 1166
frequency sensitivity 1167
205     dv = imfilter( reshape( dv0, nely, nelx ) ./ dHs, h, bcF ); % Filter volume 1168
sensitivity 1169
206     %% MMA OPTIMIZATION OF DESIGN VARIABLES 1170
207     xval = [x(:);pol(:);Ym]; % Vector of current optimization variables 1171
208     f0val = c; % Current objective function value 1172
209     df0dx = [dc(:);dp(:);dY]; % Vector of Sensitivities 1173
210     fval = [sum(xPhys(:))/(volfrac*nele) - 1;(sqrt(NATs)/sqrt(NATD))-1]; % 1174
Constraint value 1175
211     dfdx = [dv(:)' / (volfrac*nele),0*pol(:)',0;dcF(:)'/sqrt(NATD),0*pol(:)', 1176
DcF_Y(:)'/sqrt(NATD)]; % Constraint's Sensitivities 1177

```



```

1174 212 [xmma, ~, ~, ~, ~, ~, ~, ~, ~, low, upp] = mmasub(mc, nVar, loop, xval, xmin,
1175 xmax, xold1, xold2, f0val, df0dx, fval, dfdx, low, upp, a0, ai, ci, di); % MMA
1176 optimization
1177 213 xnew = reshape(xmma(1:nele,1), nely, nelx); % Vector of updated density
variable
1178 214 Density_change = max(abs(xnew(:)-x(:)));
1179 215 xold2 = xold1(:); xold1 = [x(:); pol(:); Ym];
1180 216 pol = reshape(xmma(nele+1:2*nele,1), nely, nelx); % Vector of updated
1181 polarization variables
1182 217 Ym = xmma(2*nele+1,1); % Updated mass ratio variable
1183 218 x = xnew;
1184 219 %% CONTINUATION SCHEME ON PENALIZATION FACTORS & BETA
1185 220 [penalKuu, ~] = deal(cnt(penalKuu , penalCnt, loop), cnt(beta, betaCnt, loop));
1186 221 penalKup=penalKuu*penalratio_up; penalKpp=penalKuu*penalratio_pp;
1187 222 %% PLOT DENSITIES & POLARIZATION
1188 223 figure(1); colormap(gray); imagesc(1-x); caxis([0 1]); axis equal; axis off;
drawnow;
1189 224 figure(2); colormap(jet); imagesc(((x.*(pol*2-1))+1)/2); caxis([0 1]); axis
1190 equal; axis off; drawnow;
1191 225 fprintf(' It:%2.0i Time:%3.2fs Obj:%3.4f Wm.:%3.4f We.:%3.4f Freq:%3.3f Ym
1192 .:%3.3f Vol:%3.3f ch:%3.3f\n ', loop, toc, c, Wm, We, Freq, Ym, mean(xPhys(:)),
1193 Density_change);
1194 226 end
1195 227 % ||=====||
1196 228 % || THIS CODE IS WRITTEN BY ABBAS HOMAYOUNI-AMLASHI, THOMAS SCHLINQUER, ||
1197 229 % || Peter Kipkemoi, Jean Bosco Byiringiro, MICKY RAKOTONDRABE, ||
1198 230 % || Michael Gauthier and ABDENBI MOHAND-OUAID. January 2024. ||
1199 231 % ||=====||
1200
1201
1202
1203
1204
1205
1206
1207
1208
1209
1210
1211
1212
1213
1214
1215
1216
1217
1218
1219
1220
1221
1222
1223
1224

```

References

- [1] S. Régnier, N. Chaillet, *Microrobotics for Micromanipulation* (Wiley-ISTE, publisher, 2010)
- [2] T. Schlinquer, A. Mohand-Ousaid, M. Rakotondrabe, Optimal design of a unimorph piezoelectric cantilever devoted to energy harvesting to supply animal tracking devices. *IFAC-PapersOnLine* **50**(1), 14600–14605 (2017)
- [3] S. Adali, J.C. Bruch Jr., I.S. Sadek, J.M. Sloss, Robust shape control of beams with load uncertainties by optimally placed piezo actuators. *Structural and Multidisciplinary Optimization* **19**(4), 274–281 (2000). <https://doi.org/10.1007/s001580050124>. URL <https://doi.org/10.1007/s001580050124>
- [4] A.M. Sadri, J.R. Wright, R.J. Wynne, Modelling and optimal placement of piezoelectric actuators in isotropic plates using genetic algorithms. *Smart Materials and Structures* **8**(4), 490 (1999). <https://doi.org/10.1088/0964-1726/8/4/306>. URL <https://dx.doi.org/10.1088/0964-1726/8/4/306>
- [5] M. Rakotondrabe, S. Khadraoui, *Design of Piezoelectric Actuators with Guaranteed Performances Using the Performances Inclusion Theorem* (Springer New York, New York, NY, 2013), pp. 41–59. https://doi.org/10.1007/978-1-4614-6684-0_3. URL https://doi.org/10.1007/978-1-4614-6684-0_3
- [6] S. Khadraoui, M. Rakotondrabe, P. Lutz, Optimal design of piezoelectric cantilevered actuators with guaranteed performances by using interval techniques. *IEEE/ASME Transactions on Mechatronics* **19**(5), 1660–1668 (2014)
- [7] M. Grossard, C. Rotinat-Libersa, N. Chaillet, in *2007 IEEE/ASME international conference on advanced intelligent mechatronics* (2007), pp. 1–6. <https://doi.org/10.1109/AIM.2007.4412553>
- [8] M. Grossard, C. Rotinat-Libersa, N. Chaillet, M. Boukallel, Mechanical and control-oriented design of a monolithic piezoelectric microgripper using a new topological optimization method. *IEEE/ASME Transactions on Mechatronics* **14**(1), 32–45 (2009)
- [9] M. Bendsøe, O. Sigmund, *Topology optimization. Theory, methods, and applications. 2nd ed., corrected printing* (2004). <https://doi.org/10.1007/978-3-662-05086-6>
- [10] O. Sigmund, A 99 line topology optimization code written in matlab. *Structural and multidisciplinary optimization* **21**(2), 120–127 (2001)
- [11] E. Andreassen, A. Clausen, M. Schevenels, B. Lazarov, O. Sigmund, Efficient topology optimization in matlab using 88 lines of code. *Struct Multidiscip Optim* **43**(1), 1–16 (2011)
- [12] D. Ruiz, O. Sigmund, Optimal design of robust piezoelectric microgrippers undergoing large displacements. *Structural and Multidisciplinary Optimization* **57**, 1–12 (2018). <https://doi.org/10.1007/s00158-017-1863-5>
- [13] A. Homayouni-Amlashi, T. Schlinquer, A. Mohand-Ousaid, M. Rakotondrabe, 2d topology optimization matlab codes for piezoelectric actuators and energy harvesters. *Structural and Multidisciplinary Optimization* pp. 1–32 (2020)
- [14] C. Wang, Z. Zhao, M. Zhou, O. Sigmund, X.S. Zhang, A comprehensive review of educational articles on structural and multidisciplinary optimization. *Structural and Multidisciplinary Optimization* **64**(5), 2827–2880 (2021)
- [15] A. Homayouni-Amlashi, T. Schlinquer, A. Mohand-Ousaid, M. Rakotondrabe, 2D topology optimization MATLAB codes for piezoelectric actuators and energy harvesters. *Structural and Multidisciplinary Optimization* p. 0 (2020). <https://doi.org/10.1007/s00158-020-02726-w>. URL <https://hal.archives-ouvertes.fr/hal-03033055>

- 1276 [16] T. Schlinquer, A. Homayouni-Amlashi,
1277 M. Rakotondrabe, A.M. Ousaid, Design of
1278 piezoelectric actuators by optimizing the
1279 electrodes topology. *IEEE Robotics and
1280 Automation Letters* **6**(1), 72–79 (2020)
1281
1282 [17] A.A.N. Standard, Ieee standard on piezoelec-
1283 tricity. *IEEE Transactions on Sonics and
1284 Ultrasonics* **31**(2) (1984). [https://doi.org/10.
1285 1109/T-SU.1984.31464](https://doi.org/10.1109/T-SU.1984.31464)
1286
1287 [18] R. Lerch, Simulation of piezoelectric devices
1288 by two-and three-dimensional finite elements.
1289 *IEEE transactions on ultrasonics, ferro-
1290 electrics, and frequency control* **37**(3), 233–
1291 247 (1990)
1292
1293 [19] S. Dong, Review on piezoelectric, ultrasonic,
1294 and magnetoelectric actuators. *Journal of
1295 Advanced Dielectrics* **2**, 1230001 (2012)
1296
1297 [20] M. Grossard, C. Rotinat-Libersa, N. Chail-
1298 let, M. Boukallel, Mechanical and control-
1299 oriented design of a monolithic piezoelectric
1300 microgripper using a new topological opti-
1301 mization method. *IEEE/ASME Transactions
1302 on Mechatronics* **14**(1), 32–45 (2009)
1303
1304 [21] M.P. Bendsoe, O. Sigmund, *Topology opti-
1305 mization: theory, methods, and applications*
1306 (Springer Science & Business Media, 2003)
1307
1308 [22] J.Y. Noh, G.H. Yoon, Topology optimiza-
1309 tion of piezoelectric energy harvesting devices
1310 considering static and harmonic dynamic
1311 loads. *Advances in Engineering Software* **53**,
1312 45–60 (2012)
1313
1314 [23] M. Kögl, E.C. Silva, Topology optimization
1315 of smart structures: design of piezoelectric
1316 plate and shell actuators. *Smart materials
1317 and Structures* **14**(2), 387 (2005)
1318
1319 [24] B. Zhu, X. Zhang, H. Zhang, J. Liang,
1320 H. Zang, H. Li, R. Wang, Design of compliant
1321 mechanisms using continuum topology opti-
1322 mization: A review. *Mechanism and Machine
1323 Theory* **143**, 103622 (2020)
1324
1325
1326
[25] K. Svanberg, The method of moving asymp-
totes—a new method for structural opti-
mization. *International journal for numeri-
cal methods in engineering* **24**(2), 359–373
(1987)
[26] K. Svanberg, Mma and gmma-two methods
for nonlinear optimization. vol **1**, 1–15 (2007)
[27] A.A. Babayo, M.H. Anisi, I. Ali, A review
on energy management schemes in energy
harvesting wireless sensor networks. *Renew-
able and Sustainable Energy Reviews* **76**,
1176–1184 (2017)
[28] R. Salazar, G. Taylor, M. Khalid,
A. Abdelkefi, Optimal design and energy
harvesting performance of carangiform fish-
like robotic system. *Smart Materials and
Structures* **27**(7), 075045 (2018)
[29] A. Homayouni-Amlashi, A. Mohand-Ousaid,
M. Rakotondrabe, Topology optimization
of 2dof piezoelectric plate energy harvester
under external in-plane force. *Journal of
Micro-Bio Robotics* pp. 1–13 (2020)
[30] A. Homayouni-Amlashi, A. Mohand-Ousaid,
M. Rakotondrabe, Multi directional piezo-
electric plate energy harvesters designed by
topology optimization algorithm. *IEEE
Robotics and Automation Letters* (2019)
[31] A. Homayouni-Amlashi, A. Mohand-Ousaid,
M. Rakotondrabe, Analytical modelling and
optimization of a piezoelectric cantilever
energy harvester with in-span attachment.
Micromachines **11**(6), 591 (2020)
[32] S. Wen, Z. Wu, Q. Xu, Design of a novel
two-directional piezoelectric energy harvester
with permanent magnets and multistage
force amplifier. *IEEE Transactions on Ultra-
sonics, Ferroelectrics, and Frequency Control*
67(4), 840–849 (2019)
[33] Z. Wu, Q. Xu, Design and development of
a novel two-directional energy harvester with
single piezoelectric stack. *IEEE Transactions
on Industrial Electronics* **68**(2), 1290–1298
(2020)

- [34] B. Zheng, C.J. Chang, H.C. Gea, Topology optimization of energy harvesting devices using piezoelectric materials. *Structural and Multidisciplinary Optimization* **38**(1), 17–23 (2009)
- [35] T. Schlienger, A. Mohand-Ousaid, M. Rakotondrabe, in *IEEE ICRA* (2018), pp. 1–7
- [36] B. Yang, C. Cheng, X. Wang, Z. Meng, A. Homayouni-Amlashi, Reliability-based topology optimization of piezoelectric smart structures with voltage uncertainty. *Journal of Intelligent Material Systems and Structures* **33**(15), 1975–1989 (2022)
- [37] A. Homayouni-Amlashi, M. Rakotondrabe, A. Mohand-Ousaid, in *2023 IEEE International Conference on Robotics and Automation (ICRA)* (IEEE, 2023), pp. 5426–5432
- [38] A. Erturk, D.J. Inman, *Piezoelectric energy harvesting* (John Wiley & Sons, 2011)
- [39] X. Huang, Z. Zuo, Y. Xie, Evolutionary topological optimization of vibrating continuum structures for natural frequencies. *Computers & structures* **88**(5-6), 357–364 (2010)
- [40] N.L. Pedersen, Maximization of eigenvalues using topology optimization. *Structural and multidisciplinary optimization* **20**(1), 2–11 (2000)
- [41] E. Andreassen, A. Clausen, M. Schevenels, B.S. Lazarov, O. Sigmund, Efficient topology optimization in matlab using 88 lines of code. *Structural and Multidisciplinary Optimization* **43**(1), 1–16 (2011)
- [42] F. Wang, B.S. Lazarov, O. Sigmund, On projection methods, convergence and robust formulations in topology optimization. *Structural and multidisciplinary optimization* **43**(6), 767–784 (2011)
- [43] F. Ferrari, O. Sigmund, A new generation 99 line matlab code for compliance topology optimization and its extension to 3d. *Structural and Multidisciplinary Optimization* **62**(4), 2211–2228 (2020)
- [44] J.E. Kim, D.S. Kim, P.S. Ma, Y.Y. Kim, Multi-physics interpolation for the topology optimization of piezoelectric systems. *Computer Methods in Applied Mechanics and Engineering* **199**(49-52), 3153–3168 (2010)
- [45] O. Sigmund, Design of multiphysics actuators using topology optimization—part ii: Two-material structures. *Computer methods in applied mechanics and engineering* **190**(49-50), 6605–6627 (2001)
- [46] D. Li, I.Y. Kim, Multi-material topology optimization for practical lightweight design. *Structural and Multidisciplinary Optimization* **58**, 1081–1094 (2018)
- [47] R. Tavakoli, S.M. Mohseni, Alternating active-phase algorithm for multimaterial topology optimization problems: a 115-line matlab implementation. *Structural and Multidisciplinary Optimization* **49**, 621–642 (2014)
- [48] A. Molter, J.S.O. Fonseca, L. dos Santos Fernandez, Simultaneous topology optimization of structure and piezoelectric actuators distribution. *Applied Mathematical Modelling* **40**(9-10), 5576–5588 (2016)
- [49] M. He, X. Zhang, L. dos Santos Fernandez, A. Molter, L. Xia, T. Shi, Multi-material topology optimization of piezoelectric composite structures for energy harvesting. *Composite Structures* **265**, 113783 (2021)